

1     **General comments for the Editor**

2  
3     The authors would like to thank the editors of the journal *Earth Surface Dynamics* for  
4     considering publishing our manuscript and for the Referees for their constructive criticism on  
5     the manuscript and their valuable suggestions on how to improve the manuscripts overall  
6     quality. The responses for each referees comments are presented in separate documents and all  
7     comments and suggestions was incorporated into the manuscript where possible. Looking at  
8     both the Referees comments the authors felt that we should add a joint response that would  
9     alleviate some common concerns from the referees.

10    The main objective of this manuscript was to introduce the new coupled soilscape-landform  
11    evolution model. However we strongly felt that there should be some applications of the model  
12    albeit simple, to show how the model performed well in reality and to highlight some of the  
13    geomorphic signatures emerging from the modelling results itself. We recognise that it is not a  
14    reasonable application that necessarily be directly applicable in the field setting. However we  
15    are inspired by the early work on hillslope geomorphology by authors such as *Kirkby* [1971]  
16    and *Carson and Kirkby* [1972] which was very useful in understanding hillslope evolution  
17    processes. So as first step we used a 1Dimensional hillslope to run our simulations because,  
18    understanding dynamics of 1D hillslope evolution is easier and we can better illustrate possible  
19    implications for different processes.

20    In this manuscript emphasis was given to the presenting the model formulation and only limited  
21    comparison was done with field data mainly because we were unable to find any experimental  
22    work done by any other researcher which has used a similar setup as our simulations. However  
23    a subsequent paper will deal with implications of model results in terms of one-dimensional  
24    and three-dimensional alluvial fans. In this future manuscript, we compare and contrast the  
25    model results with experimental work done by authors such as *Seal et al.* [1997], *Toro-Escobar*  
26    *et al.* [2000] and general observations done regarding naturally occurring alluvial fans and their  
27    formation dynamics.

28    We admit that the model is limited in its scientific scope. The model is based on physical  
29    fragmentation of parent soil particles and it does not model chemical transformations. The  
30    modelling approach used here is complimentary to the chemical weathering modelling work  
31    done by Michael J Kirkby [Kirkby, 1977; 1985; 2018]. However we will be incorporating a  
32    physically based chemical weathering model described by Willgoose [2018] into SSSAPAM  
33    in the future.

34    At the current time we decided not to consider SOC and its influence in the soil formation and  
35    evolution processes. All available evidence suggests that in order to effectively model SOC, it  
36    will require an extremely complicated coupled model with soil grading, soil moisture, SOC as  
37    well as vegetation. Although formulating such a model is very desirable (and would be an  
38    important endeavour by itself) for the entire scientific community, it is well beyond the scope  
39    of this current research work.

40 The deposition model of SSSPAM is designed in such a way that the difference between the  
41 transport capacity and the sediment load of the flow is always deposited regardless of the  
42 settling velocities. This is done to prevent the flow from being over the transport capacity.  
43 Depending on the material grading distribution and the concentration in the profile of the flow,  
44 the theoretical amount of the material that can be deposited can be different. In this model  
45 formulation we assume that the sediment grading is uniform and the sediment concentration is  
46 also uniform within the flow. The reality may not be as simple as that. There is literature that  
47 argues that the sediment concentration profile has an exponential distribution (i.e. most of the  
48 sediment are concentrated near the bottom of the flow) such as *Agrawal et al.* [2012] and that  
49 the grading distribution profile in the flow is also a function of the settling velocity of different  
50 particles (i.e. Larger particles are concentrated near the bottom of the flow). So in practice the  
51 amount of material deposited at each pixel according to the critical immersion depth might be  
52 higher. Although the approach used in SSSPAM may not perfectly mimic the natural behaviour  
53 of sediment deposition we believe that this is the most effective way to numerically represent  
54 this process in the model at this time.

#### 55 References.

- 56 Agrawal, Y. C., O. A. Mikkelsen, and H. Pottsmith (2012), Grain size distribution and sediment  
57 flux structure in a river profile, measured with a LISST-SL Instrument, *Sequoia Scientific, Inc.*  
58 *Report*.
- 59 Carson, M. A., and M. J. Kirkby (1972), Hillslope form and process.
- 60
- 61 Kirkby, M. (1971), Hillslope process-response models based on the continuity equation, *Inst.*  
62 *Br. Geogr. Spec. Publ*, 3(1), 5-30.
- 63
- 64 Kirkby, M. (1977), Soil development models as a component of slope models, *Earth surface*  
65 *processes*, 2(2-3), 203 -230.
- 66
- 67 Kirkby, M. (1985), A basis for soil profile modelling in a geomorphic context, *Journal of Soil*  
68 *Science*, 36(1), 97-121.
- 69
- 70 Kirkby, M. (2018), A conceptual model for physical and chemical soil profile evolution,  
71 *Geoderma*.
- 72
- 73 Seal, R., C. Paola, G. Parker, J. B. Southard, and P. R. Wilcock (1997), Experiments on  
74 downstream fining of gravel: I. Narrow-channel runs, *Journal of hydraulic engineering*,  
75 123(10), 874-884.
- 76
- 77 Toro-Escobar, C. M., C. Paola, G. Parker, P. R. Wilcock, and J. B. Southard (2000),  
78 Experiments on downstream fining of gravel. II: Wide and sandy runs, *Journal of Hydraulic*  
79 *Engineering*, 126(3), 198-208.
- 80 Willgoose, G. (2018), *Principles of Soilscape and Landscape Evolution*, Cambridge University  
81 Press.

82

83

84 **Reply for the comments from P.A. Finke (Referee #1) in italic font**

85 Journal: ESurf Title: A coupled soilscape-landform evolution model: Model formulation  
86 and initial results Author(s): W. D. Dimuth P. Welivitiya et al. MS No.: esurf-2018-16

87

88 General Comments

89 The authors describe a quantitative model suitable to estimate evolution of some soil  
90 physical properties over the landscape. The model description and the presented  
91 mathematical formulations look OK. The manuscript is well-written. My major  
92 comments relate to the over-selling of the model as a pedogenesis model (see comment  
93 1), to the linkage to the real world (2, 3) and to the clarity of model assumptions (4).

94 *General Reply*

95 *First of all the authors would like to thank the referees for expending their valuable time*  
96 *and energy to review our manuscript. We also greatly appreciate the constructive*  
97 *criticism and the comments of the referees. Referee #1 has raised 4 main issues regarding*  
98 *the current version of the manuscript. The authors will consider all the comments and*  
99 *suggestions made by the referees and accommodate them in the manuscript wherever it is*  
100 *possible. Authors response for each specific comment is presented under each referee*  
101 *comment.*

102 1. One major comment, even an objection that I have is that the paper states at many  
103 locations that it concerns a soil genesis model. This illustrates a narrow vision on soil  
104 genesis, and comes entirely from a geomorphological perspective. In fact, only soil  
105 physical processes are considered, and not even all of these (e.g. heat flow and clay  
106 migration are no part of the model, the effect of SOC on erodibility is unaccounted for).  
107 It ignores that soil genesis involves many other processes, of mineralogical, chemical  
108 and biological kinds. See Bockheim and Gennadiyev (2000) for a list of soil formation  
109 processes and Minasny et al. (2015; Fig.5) for a check if these processes are covered by  
110 the soil models of to date. I therefore advise the authors to be clear in the ambi- tion  
111 level of this model, which is the mechanistic simulation of 3D-redistribution of soil  
112 particles of various size over the landscape. Mention perhaps “soil texture evolution  
113 model”, but not soil evolution model s.l.

114 *The authors do agree with the Referee #1s comment that only limited soil formation*  
115 *processes has been considered in SSSPAM. The model is based on physical*  
116 *fragmentation of parent soil particles and it does not model chemical transformations.*  
117 *The modelling approach used here is complimentary to the chemical weathering*  
118 *modelling work done by Michael J Kirkby [Kirkby, 1977; 1985; 2018]. However we*  
119 *will be incorporating a physically based chemical weathering model described by*  
120 *Willgoose [2018] into SSSAPAM in the future. Also at the current time we decided not*  
121 *to consider SOC and its influence in the soil formation and evolution processes. All*  
122 *available evidence suggests that in order to effectively model SOC, it will require an*  
123 *extremely complicated coupled model with soil grading, soil moisture, SOC as well as*  
124 *vegetation. Although formulating such a model is very desirable for the entire scientific*  
125 *community, it is well beyond the scope of this current research work. Considering the*  
126 *Referee #1s comment and the limited number of soil formation processes simulated in*  
127 *the model we have decided to use “Soil grading evolution” model instead of*

128 “pedogenesis” model

129 2. The evolution of the soilscape is only to a limited degree connected to physical boundary  
130 conditions such as rain, evaporation, heat/temperature. As I understand it, water plays a  
131 role to redistribute topsoil material, but does not influence the subsoil (linkages to  
132 weathering of minerals, clay migration). The weathering mechanism entirely concerns  
133 physical weathering, and the process is driven by 2 parameters  $n$  and  $\alpha$ , which are  
134 empirical (section 2.4). True drivers of physical weathering are related to temperature  
135 fluctuations, and specifically the occurrence of frost. For these reasons the model is not  
136 fully mechanistic, i.e. does not represent the actual processes, but rather “functional”, it  
137 describes what happens and uses empirical factors to achieve this. This means that the  
138 model cannot be used for studies on effects of global change on soilscales, where  
139 differences in P, PE and T should drive the processes. I would invite the authors to  
140 discuss this item in the paper.

141

142 *The authors believe that the Referee #1 may have misunderstood the complexity of the*  
143 *weathering mechanism and how the weathering rate of each soil layer at each pixel*  
144 *(node) is calculated due to the concise manner which it is presented. The 2 parameters*  
145 *mentioned by the Referee #1 only controls the weathering geometry (how many*  
146 *daughter particles and their relative sizes) the weathering rate of each soil layer is*  
147 *controlled by the depth dependent weathering function. The rationale behind these*  
148 *depth dependent weathering functions and how they relate to the “drivers of the*  
149 *physical weathering (specially temperature fluctuations through the soil profile)” are*  
150 *extensively described in Welivitiya et al.[2016]. The authors decided not to repeat the*  
151 *material in previously mentioned paper here due to manuscript length concerns. Also*  
152 *SSSPAM is capable of using depth dependent weathering functions for each simulation*  
153 *node (pixel) depending on the geographical distribution of various physical weathering*  
154 *drivers such as temperature. Also a slight modification to the weathering module in*  
155 *SSSPAM will be able to simulate temporal variations of these weathering drivers as*  
156 *well. So SSSPAM can actually be used to study the effects of global change on soilscales*  
157 *in the future. For the initial simulations the authors decided to keep the simulation setup*  
158 *as simple as possible to better observe and study how the core parts of the models*  
159 *perform and to see whether the results reflect general trends observed on hillslopes in*  
160 *nature. In later stages more and more capabilities of SSSPAM will be activated and a*  
161 *wide range of multidimensional soilscale simulations will be possible. As the Referee*  
162 *#1 suggests a small paragraph is added to the section to state this fact.*

163 3. To allow model testing beyond plausibility testing (“face validity”), which is attempted  
164 in the paper, additionally, confrontation to field data would be needed. This is clearly  
165 beyond the scope of this paper and, unfortunately, of most soilscale modelling studies.  
166 Some sensitivity experiments are done in this paper, which is commendable. I would  
167 expect a strong sensitivity of projected landscapes to the initial landscape as well, but  
168 this was not studied. This again touches the ambition level of this model: is it meant for  
169 synthetic studies or for real world cases?

170 *The authors appreciate the Referee #1s understanding and grasp of the practical*  
171 *difficulties of comparing results produced through a model like SSSPAM with field data.*  
172 *The authors do agree that the simulations presented in this manuscript concerns a*

173 *hypothetical situation and not much attention was made to compare results with real*  
174 *world scenarios. However the main objective of this manuscript was to introduce the*  
175 *new coupled soilscape-landform evolution model and demonstrate its ability to co*  
176 *evolve soilscape and landform together resulting in real world trends. So to keep the*  
177 *focus of this manuscript to the model development and model mechanics and to keep*  
178 *the manuscript at a reasonable size, the authors decided not to include a result*  
179 *comparison section to the current manuscript. In fact we have already done some*  
180 *comparison studies of the model simulations (particularly the deposition region of the*  
181 *landforms) with experimental flume scale studies and fluvial fan development and the*  
182 *simulations will be published in 1 or 2 separate manuscripts in the near future. In these*  
183 *simulations we have identified that the model (even with a reasonable synthetic setup)*  
184 *was able to generate similar trends identified in nature in terms of particle size*  
185 *distribution and landform morphology (particularly for alluvial fans). So we believe*  
186 *that although highly simplified in terms of the number of pedogenetic processes, the*  
187 *model still can be used to explore real world cases.*

188 4. In general, some assumptions are not so clear. For instance: how does mass  
189 redistribution relate to the elevation of the soil-atmosphere interface, in other words,  
190 how are mass and volume connected. OK, via the bulk density (for erosion in eq.4; for  
191 deposition in eq. 7), but is bulk density then assumed a constant and not affected by  
192 bioturbation, strain by weathering? Is this valid over 60.000 years? Are there other  
193 assumptions that should be known?

194 *The authors agree that some assumptions made during the model development phase may*  
195 *have been omitted from the manuscript. Revised the manuscript and assumptions are*  
196 *clearly presented*

197

198 A few specifics:

199 - 1.83: "scorpan" not introduced; this is in fact clorpt+soil point data+position (see  
200 McBratney et al. 2003), thus not so different.

201 - *The authors agree that scorpan is in fact a further development of clorpt as the Refree*  
202 *#1 has pointed out. The sentence regarding scorpan was revised and the association of*  
203 *scorpan to clorpt is introduced.*

204 - 1.573: erosion and d50 correlate: is this a model artefact? For instance, if the organic  
205 matter content would be simulated as well, would it not become part of the correlative  
206 complex?

207 *Yes, all soil components are part of the correlative complex however extensive*  
208 *work has demonstrated that d50 is strongly related to erosion.. However this*  
209 *relationship may be true for natural hillslopes as well due to the process of*  
210 *armorng. i.e High erosion means ability to erode relatively large particles*  
211 *which leads to higher d50. If we incorporate the effects of SOC we would*  
212 *imagine that it will definitely come in to the correlation complex*

213 -

214 - 1.689: soil formation and its evolution?=repetition.

215 *There seems to be a repetition in processes describing soil formation and evolution. The*  
216 *sentence was reworded*

217

218 - References:

219 Bockheim, J.G., Gennadiyev, A.N., 2000. The role of soil-forming processes in the  
220 definition of taxa in Soil Taxonomy and the World Soil Reference Base. *Geoderma* 95,  
221 53–72.

222 Budiman Minasny, Peter Finke, Uta Stockmann, Tom Vanwallegem, and Alex McBrat-  
223 ney. 2015. Resolving the integral connection between pedogenesis and landscape  
224 evolution. *Earth-Science Reviews* 150: 102-12

225 Kirkby, M. (1977), Soil development models as a component of slope models, *Earth*  
226 *surface processes*, 2(2-3), 203 -230.

227 Kirkby, M. (1985), A basis for soil profile modelling in a geomorphic context, *Journal*  
228 *of Soil Science*, 36(1), 97-121.

229 Kirkby, M. (2018), A conceptual model for physical and chemical soil profile evolution,  
230 *Geoderma*.

231

232

233

234

235

236

237

238

239

240

241

242

243

244

245

246 **Reply for the comments from A.J.A.M. Temme (Referee #2) in italic font**

247  
248

249 The manuscript by Welivitiya and co-authors presents a simulation performed with their novel  
250 soil-landscape evolution model. The model and the rationale behind it are pre- sented  
251 in detail. The model simulation is on a simplified 2D landscape (i.e. a row of cells)  
252 representing a plateau over a hillslope and a valley. Two scenarios are simulated, with  
253 different depth-dependent weathering functions. Findings are discussed in details, and  
254 appear to indicate that the model functions well, and that basic expectations about the  
255 joint development of soils and landscapes (co-evolution) are met. The paper is  
256 interesting to me as a soil-landscape modeler, and I greatly enjoyed the detailed model  
257 layout and accompanying figures.

258

259 *General Reply*

260 *First of all the authors would like to thank the referees for expending their valuable time*  
261 *and energy to review our manuscript. We also greatly appreciate the constructive*  
262 *criticism and the comments of the referees very much. The authors will consider all the*  
263 *comments and suggestions made by the referees and accommodate them in the*  
264 *manuscript wherever it is possible.*

265

266 I have detailed suggestions in the attached annotations, that amount to minor revisions in and  
267 of themselves. Below, I add three general concerns.

268 1. Although the paper is very interesting to me, I am not sure that it is to the general audience  
269 of ESurfD. The meat of the paper is the model presentation, to my mind. That makes me  
270 wonder whether an outlet such as Geoscientific Model Development of Computers and  
271 Geosciences is not a better choice.

272 *The authors do agree that the main objective of this manuscript and the bulk of its*  
273 *content has to do with model formulation and implementation. If the manuscript was*  
274 *just model formulation, we would agree with the Referee #2 s suggestion on*  
275 *submitting this manuscript elsewhere which caters to more mathematically oriented*  
276 *audience. Although a manuscript concerning only model formulation may be*  
277 *interesting, we strongly felt that we needed to include some initial model results*  
278 *(albite simple) to illustrate how the model performed at the simple scale. Also we*  
279 *wanted to highlight some of the geomorphic signatures emerging from the modelling*  
280 *results itself. We believe that publication here is important for not just the modelling*  
281 *community but also for the general geomorphology and soils community who through*  
282 *this work can observe some important physical insights but also raises some*  
283 *important questions. The other important issue is that lack of field data to*  
284 *calibrate/evaluate such models. We hope that we may inspire fieldwork (or reveal*  
285 *existing data) to advance such models as that described here. With this in mind, We*  
286 *strongly believe that Earth Surface Dynamics is the better choice for publishing this*  
287 *manuscript.*

288

289 2. The simulation that illustrates the model's performance, is interesting but hypothet- ical.  
290 The paper does a great job of explaining what the results are, but does not give much attention

291 to what that means for how we should think about landscape evolution. This may be possible  
292 only in a limited way, given the hypothetical setup, but I do think some comparisons with  
293 existing thinking and findings from others are possible. I do one suggestion in the annotations.  
294 In another outlet, a lack of connection with exist- ing thinking would be no problem at all,  
295 but I think that in ESurfD the readership is particularly interested in that aspect (and perhaps  
296 less in model workings).

297 3.

298 *The authors do agree that the simulations presented in this manuscript concerns a*  
299 *hypothetical situation and not much attention was made to compare results with real*  
300 *world scenarios. As the Referee #2 has understood the main objective of this*  
301 *manuscript was to introduce the new coupled soilscape-landform evolution model and*  
302 *demonstrate its ability to co evolve soilscape and landform together resulting in real*  
303 *world trends. So to keep the focus of this manuscript to the model development and*  
304 *model mechanics and to keep the manuscript at a reasonable size, the authors decided*  
305 *not to include a result comparison section to the current manuscript. In fact we have*  
306 *already done some comparison study on the model simulations (particularly the*  
307 *deposition region of the landforms) with experimental flume scale studies and fluvial*  
308 *fan development and the results will be published in 1 or 2 separate manuscripts in*  
309 *the near future. We also highlight the issue of a lack of field data in the previous*  
310 *comment.*

311

312 4. Although the model description is detailed and accurate, it would benefit from pointing out  
313 differences with existing models or a few more tradeoffs between accuracy and efficiency,  
314 especially where some of the innovative aspects are covered. How do these differ from existing  
315 models such as Lorica? I give a few suggestions for improvement.

316 I am glad to see this work in manuscript form, and I am happy to have it in the public domain  
317 so it can be used by colleagues. I wish the authors good luck in considering the changes  
318 suggested.

319

320 Please also note the supplement to this comment:

321 [https://www.earth-surf-dynam-discuss.net/esurf-2018-16/esurf-2018-16-RC2-](https://www.earth-surf-dynam-discuss.net/esurf-2018-16/esurf-2018-16-RC2-supplement.pdf)  
322 [supplement.pdf](https://www.earth-surf-dynam-discuss.net/esurf-2018-16/esurf-2018-16-RC2-supplement.pdf)

323

324

325 ***Specific comments from the supplemental document***

326

327 Referee #2 comment Page 9: I continue to struggle with these issues myself. Propagating  
328 resupply seems perfectly reasonable, and is necessary if layer thickness/mass is constant but  
329 don't you in this way always provide the top armouring layer with easily erodible soil? I  
330 imagine the result is a less effective armour. Does this reflect the real process?

331

332 *The authors appreciate the Reviewers comments, understanding and grasp of the practical*  
333 *difficulties of material propagation in a model like SSSPAM. However according to the*  
334 *method used here the resupplied material to the armour layer is not always easily erodible.*



335 *Size selectivity only applies to the material movement from the armour layer to the flowing*  
336 *water layer above (i.e. depending on the surface water discharge rate, smaller particles are*  
337 *easily removed from the surface armour layer while larger particles remain). The material*  
338 *resupply to the surface armour occurs from the layer below and the resupplied material have*  
339 *the same grading as the subsurface layer grading (no size selectivity) so both small particles*  
340 *and large particles are resupplied to the armour layer. Most of the time the net effect of this*  
341 *material resupply and the size selective erosion will be enrichment of larger particles and*  
342 *armour strengthening. Depending on the depth dependent weathering function the relative*  
343 *coarseness of the subsurface layers can be less compared to armour layer. But once the*  
344 *armour layer is reconfigured with the added material from below and removal of small*  
345 *particles through erosion, again the net effect is armour strengthening. This layer*  
346 *restructuring is explained later in the paper.*

347

348 Referee #2 comment Page 10: If I see it correctly this all means that if you need to deposit  
349 20kg of material and all you have in transport is clays, then you'll deposit some/all of the  
350 clays right? Regardless of the settling velocity.

351

352 *Yes the referee #2 is correct in recognising this factor. If all there in the transport is clay the*  
353 *amount of material which need to be deposited will be deposited from the available clay. Size*  
354 *selectivity comes in to play when there are a range of particles in the transport (which is*  
355 *almost always the case). Then the larger particles with higher settling velocities will deposit*  
356 *first.*

357 Referee #2 comment Page 13: Ok, this makes me doubt what I said three pages ago. –at the  
358 cost of my understanding. Tell me is  $\Sigma$ deposition in a cell equal to  $L_{in} - T_c$ , which I thought  
359 before or is it dictated by the settling velocity? The later seems to allow for  $\Sigma$ deposition to be  
360  $< L_{in} - T_c$ .

361 *The Referee #2s earlier assumption is correct. The  $\Sigma$ deposition at a pixel is always equals to*  
362  *$L_{in} - T_c$ . The settling velocities and the critical immersion depths for that matter dictates the*  
363 *distribution of the deposited particles. The Referee 2 is also correct that at the first glance it*  
364 *seems like  $\Sigma$ deposition can be  $< L_{in} - T_c$ . This is why we have the adjustment vector  $K$*   
365 *(equation 5) which ensures*

366  $\Sigma$ deposition =  $L_{in} - T_c$  (always). The authors previously had a worked example on how this  
367 correction vector is calculated. However the authors thought that this may confuse readers  
368 with less mathematical/modelling experience and decided not to include it in the final version  
369 of the manuscript. The example is again added to the main body of the manuscript. Following  
370 is this omitted section with the example.

371

372

373 Calculation of deposition mass vector

374 Following simplified example shows the need to have this adjustment vector and the method  
 375 we used to calculate it.

376 **Table 2** Example calculation of adjustment vector  $\underline{K}$ .

Size Class	Elements of $\underline{\psi}_{in}$ ( $\psi_z$ )	Entries of $\underline{J}$ ( $J_{z,z}$ )	$J_{z,z} \psi_z$	Adjusted $J_{z,z} \psi_z$	Deficit / Surplus	Diagonal elements of $\underline{K}$	Entries of $\underline{\Phi}$
1	5.00	1.0	5.00	7.29	-2.29	-2.29	5.00
2	10.00	0.7	7.00	10.21	-0.21	-0.21	10.00
3	20.00	0.4	8.00	11.67	8.33	2.00	13.67
4	40.00	0.1	4.00	5.83	34.17	0.50	6.33
Total	75.00		24.00	35.00			35.00

377  
 378 Consider the example values given in Table 2. The total mass of the incoming sediments is 75  
 379 kg and the sediments are distributed in four size classes. Here the size class one is the largest  
 380 and has the highest potential for deposition (with  $J_{1,1} = 1$ ) while the size class four has the  
 381 lowest potential for deposition (with  $J_{4,4} = 0.1$ ). If the transport capacity  $T_e$  is 40 kg, 35 kg of  
 382 incoming sediments should deposit at the pixel as the total deposition  $D$ . Using the  $\sum J_{z,z} \psi_z$   
 383 value (which is 24) and rescaling these values with  $D$  (total deposition mass), we can calculate  
 384 the masses of sediments which need to be deposited from each grading class. In some cases  
 385 (when the total deposition  $D$  is higher than the  $\sum J_{z,z} \psi_z$  value) the mass of material which  
 386 needs to be deposited can be larger than the available sediments in that particular size class.  
 387 In this example there is 5 kg of sediments in the 1st size class and 10 kg of sediments in the  
 388 second size class respectively. However, our adjusted calculation dictate that there should be  
 389 7.29 kg deposition from the 1st size class and 10.21 kg from the 2nd size class which is not  
 390 possible. So these values needs to be adjusted to reflect maximum possible deposition from size  
 391 classes one and two which are 5 kg and 10 kg respectively. This adjustment introduces a deficit  
 392 of 2.5 kg to the total deposition and it needs to be deposited from the 3<sup>rd</sup> and 4<sup>th</sup> smaller grading  
 393 classes. According to the deposition matrix values  $J_{z,z}$  the deposition probability ratio between  
 394 3<sup>rd</sup> and 4<sup>th</sup> grading class is 4:1 (0.4:0.1). The deficit mass 2.5kg is deposited from the 3rd and  
 395 4th size class with 4:1 ratio which accounts to an additional deposition mass of 2 kg from 3rd  
 396 size class and 0.5 kg from the 4th size class. In this way the entries of the adjustment vector  $\underline{K}$   
 397 are calculated. Depending on the number of size classes and the distribution of the sediments,  
 398 this adjustment vector  $\underline{K}$  needs to be calculated iteratively.

399  
 400 Referee #2 comment Page 16: The section 2.3.2 feels excessively detailed and long for a  
 401 paper (Better in a model manual perhaps?) consider shortening drastically.

402 *The authors agree with Referee#2s comment regarding the section 2.3.2. The section is*  
403 *modified and some paragraphs were removed.*

404 Referee 2 comment Page 17: Also it conveniently avoid possible negative effects of d8.  
405 Please comment here, or where you present the d8 choice.

406 *At the time this manuscript was prepared, the authors had already ran the simulation for*  
407 *3dimentional synthetic landforms as well. However the authors did not find any significant*  
408 *issues with using d8 for flow calculation.*

409 Referee #2 comment Page 21: I'm trying to imagine implications. Does it follow from this  
410 that nick points cutting back into higher regions slow down less than otherwise expected  
411 since they meet fine soft soils as they proceeds further into the plateau? Please comment and  
412 harvest for your readers.

413 *The Referee #2s understanding is correct. When the erosion region cuts back in to the*  
414 *plateau area, weathering process has already broken-down the coarse material in to finer*  
415 *constituents where it can be readily eroded away by the erosion region cutting in to the*  
416 *plateau region. If we did not have weathering the rate at which the erosion region cutting*  
417 *back to the plateau region would be slower as it requires the removal of coarser soil*  
418 *particles. A small discussion mentioning this implication was added to the manuscript as per*  
419 *Referee #2s comment*

420 Referee #2 comment Page 24: I have the opinion/impression that the discussion section is  
421 quite detailed in describing your results. Perhaps a bit much so, and that there is not enough  
422 in the way of comparing dynamics with results reported by others, empirically or otherwise.

423 *As Referee #2s Comments the Discussion section is modified and some paragraphs were*  
424 *removed*

425 Referee #2 comment Page 26: It would be good to shorten conclusions to about 1/2 or 2/3 of  
426 their size.

427 *As Referee #2s Comments the conclusions section is modified and some paragraphs were*  
428 *removed*

429

430

431

432

433

434

435 **A coupled soilscape-landform evolution model: Model formulation**  
436 **and initial results.**

437

438

439

440

441 W. D. Dimuth P. Welivitiya<sup>1,2</sup>, Garry R Willgoose<sup>1</sup>, Greg R Hancock<sup>2</sup>

442 <sup>1</sup>School of Engineering, The University of Newcastle, Callaghan, 2308, Australia.

443 <sup>2</sup>School of Environment and Life Sciences, The University of Newcastle, Callaghan, 2308,  
444 Australia.

445 Corresponding Author: Garry Willgoose

446 Garry.willgoose@newcastle.edu.au

447

448

449

450

451

452

453

454

455

456 **Abstract**

457 This paper describes the coupling of the State Space Soil Production and Assessment Model  
458 (SSSPAM) soilscape evolution model with a landform evolution model to integrate soil profile  
459 dynamics and landform evolution. SSSPAM is a computationally efficient soil evolution model which  
460 was formulated by generalising the mARM3D modelling framework to further explore the soil profile  
461 self-organization in space and time, and its dynamic evolution. The landform evolution was integrated  
462 into SSSPAM by incorporating the processes of deposition and elevation changes resulting from erosion  
463 and deposition. The complexities of the physically based process equations were simplified by  
464 introducing state-space matrix methodology that allows efficient simulation of mechanistically linked  
465 landscape and pedogenesis processes for catena spatial scales. [The modelling approach and the physics](#)  
466 [underpinning the modelled processes are described in detail.](#) SSSPAM explicitly describes the particle  
467 size grading of the entire soil profile at different soil depths, tracks the sediment grading of the flow,  
468 and calculates the elevation difference caused by erosion and deposition at every point in the soilscape  
469 at each time step. The landform evolution model allows the landform to change in response to (1)  
470 erosion and deposition, and (2) spatial organisation of the co-evolving soils. This allows comprehensive  
471 analysis of soil landform interactions and soil self-organization. SSSPAM simulates fluvial erosion,  
472 armouring, physical weathering, and sediment deposition. The modular nature of the SSSPAM  
473 framework allows integration of other pedogenesis processes [in follow-on research projects to be easily](#)  
474 [incorporated.](#) This paper presents the initial results of soil profile evolution on a dynamic landform.  
475 These simulations were carried out on a simple linear hillslope to understand the relationships between  
476 soil characteristics and the geomorphic attributes (e.g. slope, area). Process interactions which lead to  
477 such relationships were also identified. The influence of the depth dependent weathering function on  
478 soilscape and landform evolution was also explored. These simulations show that the balance between  
479 erosion rate and sediment load in the flow accounts for the variability in spatial soil characteristics while  
480 the depth dependent weathering function has a major influence on soil formation and landform  
481 evolution. [The results demonstrate the ability of SSSPAM to explore hillslope and catchment scale soil](#)  
482 [and landscape evolution in a coupled framework.](#)

483

484

485

486

487

488

489

490

## 491 1. Introduction

492 Soil is one of the most important substances found on planet Earth. As the uppermost  
493 layer of the earth surface, soil supports all the terrestrial organisms ranging from microbes to  
494 plants to humans and provides the substrate for terrestrial life [Lin, 2011]. Soil provides a  
495 transport and a storage medium for water and gases (e.g. carbon dioxide which influences the  
496 global climate) [Strahler and Strahler, 2006]. The nature of the soil heavily influences both  
497 geomorphological and hydrological processes [Bryan, 2000]. In addition to the importance of  
498 soil from an environmental standpoint, it provides a basis for human civilization and played an  
499 important role in its advancement through the means of agricultural development [Jenny,  
500 1941]. Understanding the formation and the global distribution of soil (and its functional  
501 properties) is imperative in the quest for sustainable use of this resource.

502 Characterization of soil properties at a global scale by sampling and analysis is time  
503 consuming and prohibitively expensive due to the dynamic nature of the soil system and its  
504 complexity [Hillel, 1982]. However over the years researchers have found strong links between  
505 different soil properties ~~and between soil properties and~~ the geomorphology of the landform  
506 on which they reside [Gessler et al. 2000, 1995]. Working on this ~~hypothesis relationship~~  
507 several statistical methods have been developed to determine and map various soil properties  
508 depending on other soil properties and geomorphology such as pedotransfer functions,  
509 geostatistical approaches, and state-factor (e.g. CLORPT) approaches [Behrens and Scholten,  
510 2006]. Pedotransfer functions (PTFs) use easily measurable soil attributes such as particle size  
511 distribution, amount of organic matter, and clay content to predict hard to measure soil  
512 properties such as soil water content. Although very useful, PTFs need a large database of  
513 spatially distributed soil property data and require site specific calibration [Benites et al., 2007].  
514 Geostatistical methods use a finite number of field samples to interpolate the soil property  
515 distribution over a large area. Developing soil property maps using geostatistical methods ~~are~~  
516 is possible for smaller spatial scales, however soil sampling and mapping soil attributes can be  
517 prohibitively expensive and time consuming for larger spatial domains [Scull et al., 2003].  
518 State-factor methods, such as CLORPT and SCORPAN use digitized existing soil maps and  
519 easily measurable soil attributes data to generate spatially distributed soil property data using  
520 mathematical concepts such as fuzzy set theory, artificial neural network or decision tree

Commented [rc1]: CAPS?

521 methods [McBratney *et al.*, 2003]. However these techniques also suffer from scalability issues  
522 and the typical need for site specific calibration.

523 While spatial mapping of soil properties is important, understanding the evolution of  
524 these soil properties and processes responsible for observed spatial variability of soil properties  
525 is also important. In order to quantify these processes and predict the soil characteristics  
526 evolution through time, dynamic process based models are required [Hoosbeek and Bryant,  
527 1992]. These mechanistic process models predict soil properties using both geomorphological  
528 attributes and various physical processes such as weathering, erosion, and bioturbation  
529 [Minasny and McBratney, 1999]. ARMOUR developed by Sharmeen and Willgoose [2006] is  
530 one of the earliest process based pedogenesis models. ARMOUR simulated surface armouring  
531 based on erosion and size selective entrainment of sediments driven by rainfall events and  
532 overland flow, and physical weathering of the soil particles which break down the surface  
533 armour layer. However, very high computational resource requirements and long run times  
534 prevented ARMOUR from performing simulations beyond short hillslopes. Subsequently  
535 Cohen *et al.* [2009] developed mARM by implementing a state-space matrix methodology to  
536 simplify the process based equations and calibrated its process parameters using the results  
537 from ARMOUR. Its high computational efficiency allowed mARM to explore the soil  
538 evolution characteristics on spatially distributed landforms. Through their simulations Cohen  
539 *et al.* [2009] found a strong relationship between the geomorphic quantities contributing area,  
540 slope, and soil surface grading  $d_{50}$ . Both ARMOUR and mARM used two soil layers to simulate  
541 the a surface armour layer and a semi-infinite subsurface soil layer which supply supplies  
542 sediments to the upper armour layer. For this reason both of these models were incapable of  
543 exploring the evolution of the subsurface soil profiles. To overcome this limitation Cohen *et al.*  
544 *al.* [2010] developed mARM3D by incorporating multiple soil layers into mARM modelling  
545 framework. To generalise the work of Cohen *et al.* [2010], [Welivitiya *et al.*, 2016] [W-D-P  
546 Welivitiya *et al.*, 2016b] [W-D-P Welivitiya *et al.*, 2016b] [W-D-D-P Welivitiya *et al.* [2016a]  
547 developed a new pedogenesis soil grading evolution model called SSSPAM, which was based  
548 on the approach of mARM3D and showed that the area-slope- $d_{50}$  relationship in Cohen *et al.*  
549 [2009] was robust against changes in process and climate parameters and that the relationship  
550 is also true for all the subsurface soil layers, not just the surface. Although these models predict  
551 the properties of the soil profile at an individual pixel, they do not model the spatial  
552 interconnectivity between different parts of the soil catena resulting from transport-limited  
553 erosion and deposition. Lateral material movement and particle redistribution through

554 deposition is very important in determining the soil characteristics such as soil depth and soil  
555 texture [Chittleborough, 1992; Minasny and McBratney, 2006]. In order to correctly predict  
556 ~~the~~ spatially distributed soil attributes and determine the changes in soil attributes with time,  
557 coupling soil profile evolution with landform evolution is important.

558 The first attempt ~~on to~~ integrating soilscape evolution with landform evolution was  
559 done by Minasny and McBratney [1999; 2001]. They used a single layer to model the influence  
560 of soil and weathering processes on landform evolution. In addition to Minasny and McBratney  
561 [1999; 2001] there are a number of conceptual frameworks found in literature for developing  
562 coupled soil profile-landform evolution models [Sommer *et al.*, 2008; Yoo and Mudd, 2008].  
563 MILESD [Vanwalleghe *et al.* [2013] is a model which can simulate soil profile evolution  
564 coupled with landform evolution. MILESD is built upon the conceptual framework of  
565 landscape-scale models for soil redistribution by Minasny and McBratney [1999; 2001] and  
566 pedon-scale soil formation model developed by Salvador-Blanes *et al.* [2007]. In MILESD the  
567 soil profile is divided into four layers containing the bottommost bedrock layer and 3 soil layers  
568 above it representing the A, B, and C soil horizons. MILESD was used to model soil  
569 development over 60,000 years for a field site in Werrikimbe National Park, Australia  
570 [Vanwalleghe *et al.*, 2013]. They matched trends observed in the field such as the spatial  
571 variation of soil thickness, soil texture and organic carbon content. A limitation of MILESD is  
572 that it only uses three layers to represent the soil profile. Recently the soil evolution module  
573 used in MILESD has been modified to incorporate additional layers and has been combined  
574 with the landform evolution model LAPSUS to develop a new coupled soilscape-landform  
575 evolution model, LORICA [Temme and Vanwalleghe, 2015]. They found similar results for  
576 soil-landform interaction and evolution similar to MILESD simulation results.

577 Since only three layers were used in MILESD, the representation of the particle size  
578 distribution down the soil profile was limited. Although LORICA incorporated additional soil  
579 layers into the MILESD modelling framework, detailed exploration of soil profile evolution or  
580 interactions between landform evolution and soil profile evolution has not yet been done with  
581 this model. Importantly, particle size distribution of the soil can be used as a proxy for various  
582 soil attributes such as the soil moisture content [Arya and Paris, 1981; Schaap *et al.*, 2001].  
583 The main objective of this paper is to present a new soilscape evolution model capable of  
584 predicting the particle size distribution of the entire soil profile by integrating a previously  
585 developed pedogenesissoil grading evolution model in to a landscape evolution model.



586 In previous papers we have presented a pedogenesis model (on a fixed elevation  
587 landform) called State Space Soil Production Assessment Model (SSSPAM) [Welivitiya et al.,  
588 2016] and explored relationships between the geomorphic parameters slope, contributing area  
589 and the soil grading distribution. Similar to previous pedogenesis models such as mARM3D  
590 [Cohen et al., 2009; 2010], SSSPAM did not consider the interconnectivity between evolving  
591 soil pedons through fluvial processes, no landform evolution was modelled and no changes in  
592 the contributing area and slope occurred. ~~Here~~In this paper we present the methodology for  
593 incorporating sediment transport, deposition and elevation changes of the landform in to  
594 SSSPAM modelling framework to create a coupled soilscape-landform evolution model.  
595 Detailed information regarding the development and testing of SSSPAM ~~pedogenesissoil~~  
596 ~~grading evolution~~ model is provided in previous papers by the authors ([Cohen et al., 2010; W  
597 D D P Welivitiya et al., 2016a][Sagy Cohen et al., 2010; W D P Welivitiya et al., 2016b][Cohen  
598 et al., 2010; W D P Welivitiya et al., 2016b][Cohen et al., 2010; W D P Welivitiya et al.,  
599 2016b][Cohen et al., 2010; Welivitiya et al., 2016]). The main focus of this paper is to  
600 incorporate landform evolution into the SSSPAM framework. In addition to the model  
601 development we also present the initial results of coupled soilscape-landform evolution  
602 exemplified on a linear hillslope.

## 603 2. Model development.

604 The introduction of a landform into the SSSPAM framework is done using a digital  
605 elevation model. The structure of the landform evolution model follows that for transport-  
606 limited erosion [Willgoose et al., 1991] but modified so as to facilitate its coupling with the  
607 soilscape ~~pedogenesissoil~~ ~~grading evolution~~ model SSSPAM described in [W D D P Welivitiya  
608 et al., 2016a][Welivitiya et al., 2016]. Here a regular square grid digital elevation model was  
609 used and converted ~~it~~ into a two dimensional array which can be easily processed and analysed  
610 in the Python/Cython programming language. Using the “steepest-slope” ~~criteria~~ ~~criterion~~  
611 [Tarboton, 1997] the flow direction and the slope value of the each pixel was determined. Then  
612 using the created flow direction matrix, the contributing area of each pixel was determined  
613 using the “D8” method [O’Callaghan and Mark, 1984] with a recursive algorithm.

614 The soil profile evolution of each pixel is determined using the interactions between  
615 the soil profile and the flowing water at the surface. Figure 1 shows these layers and their  
616 potential interactions. This is similar to the schematic for the standalone ~~pedogenesissoil~~  
617 ~~grading evolution~~ model but is different in that the erosion/deposition at the surface is a result

618 of the imbalance between upslope and downslope sediment transport. The water layer acts as  
619 the medium in which soil particle entrainment or deposition occurs depending on the transport  
620 capacity of the water at that pixel. The water provides the lateral coupling across the landform,  
621 by the sediment transport process. The soil profile is modelled as several layers to reflect ~~on~~  
622 the fact that the soil grading changes with soil depth depending on the weathering  
623 characteristics of soil. Erosion of soil and/or sediment deposition occurs at the surface soil layer  
624 (surface armour layer).

625 SSSPAM uses the state-space matrix approach to evolve the soil grading through the  
626 soil profile. The state-space matrix methodology used for soilscape evolution is presented in  
627 detail elsewhere [Cohen *et al.*, 2009; 2010; Welivitiya *et al.*, 2016] and will not be discussed in  
628 detail here. Using this method a range of processes (e.g. erosion, weathering, deposition) can  
629 be represented and applied so that the total change of soil layers and their properties can be  
630 determined [Cohen *et al.*, 2009; 2010]. Once the erosion and deposition mass is determined,  
631 ~~the~~ elevation changes are calculated and the digital elevation model ~~was~~ is modified  
632 accordingly. Once the algorithm completes modifying the digital elevation model matrix, the  
633 calculation of flow direction and ~~contribution~~ contributing area is done and the process is  
634 repeated until a given number of iterations (evolution time) is reached.

## 635 2.1 Characterizing erosion and deposition.

636 As described in Welivitiya *et al.* [2016], the SSSPAM ~~pedogenesis~~ soil grading  
637 evolution model used ~~a~~ detachment-limited erosion model to calculate the amount of erosion.  
638 In order to simulate deposition and to differentiate between erosion and deposition, a transport-  
639 limited model is incorporated into the ~~pedogenesis~~ soil grading evolution model SSSPAM.  
640 Before calculating the erosion or deposition at a pixel (i.e. grid cell/node) we determine the  
641 transport capacity of the flow at that particular pixel. The transport capacity determines if the  
642 pixel is being subjected to erosion or deposition. The calculation of the transport capacity at  
643 each pixel is done according to the empirical equation presented by Zhang *et al.* [2011] which  
644 was determined by ~~their~~ flume scale sediment detachment experiments. The transport capacity  
645 at a pixel (node)  $T_c$  (kg/s) is given by,

$$646 T_c = \left( K_1 Q^{\delta_1} S^{\delta_2} d_{50a}^{\delta_3} \right) \omega \quad (1)$$

647 where  $Q$  is the discharge per unit width ( $\text{m}^3/\text{s}/\text{m}$ ) at the pixel,  $S$  is the slope gradient ( $\text{m}/\text{m}$ ) and  
 648  $d_{50a}$  is the median diameter of the sediment load in the flow ( $\text{m}$ ),  $K_1$ ,  $\delta_1$ ,  $\delta_2$ ,  $\delta_3$  are constants  
 649 determined empirically and  $\omega$  is the flow width ( $\text{m}$ ) at the pixel.  $Q$  is

$$650 \quad Q = \frac{rA_c}{\omega} \quad (2)$$

651 where  $r$  is runoff excess generation ( $\text{m}^3/\text{s}/\text{m}^2$ ) and  $A_c$  is contributing area ( $\text{m}^2$ ) of that pixel.  
 652 Using their flume particle detachment experiments *Zhang et al.* [2011] determined that  
 653  $K_1 = 2382.32$ ,  $\delta_1 = 1.269$ ,  $\delta_2 = 1.637$ , and  $\delta_3 = -0.345$  gave the best fit to their experimental  
 654 results (with an  $R^2$  value of 0.98). If  $\psi_{in}$  is the mass vector of the incoming sediment to the  
 655 pixel, then  $L_{in} = \sum(\psi_{in_1}, \psi_{in_2} \dots \dots \dots \psi_{in_n})$  (where  ~~$\psi_{in_x}, \psi_{in_z} \dots \dots \dots \psi_{in_x}$  are the~~  
 656 ~~elements of incoming sediment mass vector  $\psi_{in}$~~ ) is the total mass of incoming sediments to  
 657 that pixel transported by water. Here  $\psi_{in}$  represents the cumulative outflow sediment mass  
 658 vectors of upstream pixels ( $\sum \psi_{out}$ ) which drain into the pixel in question and is determined  
 659 using the flow direction matrix mentioned earlier. Using this method, SSSPAM can model the  
 660 total mass of the eroded sediment as well as the grading of the eroded material (note that  
 661 ~~elements of incoming sediment mass vector,  $\psi_{in_x}$  represents the sediment grading of the~~  
 662 ~~particle size class  $j$ .~~). Depending on the total incoming sediment load at the pixel,  $L_{in}$ , the  
 663 transport capacity  $T_c$  of the flow and the potential total erosion mass  $E_p$ , the amount of actual  
 664 erosion  $E_a$  ( $\text{kg}/\text{s}$ ) or deposition  $D$  ( $\text{kg}/\text{s}$ ) can be determined according to Table 1. ~~Here~~  
 665  ~~$\psi_{in}$  represents the cumulative outflow sediment mass vectors of upstream pixels ( $\sum \psi_{out}$ )~~  
 666 ~~which drain into the pixel in question and is determined using the flow direction matrix~~  
 667 ~~mentioned earlier.~~ The scenario (A) and (B) (in Table 1) leads to erosion and armouring while  
 668 scenario (C) leads to deposition.

Formatted: Superscript

## 669 2.2 Erosion, armouring and soil profile restructuring

670 The calculation of potential erosion  $E_p$  and armouring of the soil surface is done as in  
 671 *Welivitiya et al.* [2016] and *Cohen et al.* [2009]. The actual erosion  $E_a$  is then determined by  
 672 adjusting the potential erosion  $E_p$  according to scenarios A or B (Table 1). When calculating  
 673 the actual erosion  $E_a$  we determine only the total mass of the erodible material (although it  
 674 should be remembered that total erosion is a function of the transport capacity and that which  
 675 is in turn a function of the grading  $d_{50}$ ). The actual erosion mass vector  $G_e$  is determined using

676 the total soil surface mass grading vector  $\underline{G}$  and erosion transition matrix  $\mathbf{A}$ . The method  
 677 utilized to generate this erosion transition matrix  $\mathbf{A}$  is identical to that described in detail in  
 678 *Welivitiya et al.* [2016] and *Cohen et al.* [2009] and will not be discussed in detail here. Briefly,  
 679 the methodology is a size selective entrainment of soil particles from the surface due to erosion  
 680 leaving the surface armour layer enriched with coarser material. It is similar to the approach of  
 681 *Parker and Klingeman* [1982] which *Willgoose and Sharmeen* [2006] showed was the best fit  
 682 to their field data for their ARMOUR surface armouring model. The eroded material is added  
 683 to the sediment load flowing into the pixel and can be given as the outflow sediment mass  
 684 vector  $\underline{\psi}_{out}$ .

$$685 \quad \underline{\psi}_{out} = \underline{\psi}_{in} + \underline{G}_e \quad (3)$$

686 The actual depth of erosion  $\Delta h_E$  (m) is calculated using the equation,

$$688 \quad \Delta h_E = \frac{E_a}{R_x R_y \rho_s} \quad (4)$$

687  
 689 where  $R_x$  and  $R_y$  are the grid cell dimensions (m) in the two cardinal direction (pixel  
 690 resolution), and  $\rho_s$  is the bulk density of the soil material ( $\text{kg/m}^3$ ). Here we assume that the  
 691 bulk density  $\rho_s$  remains constant regardless of the soil grading and over the simulation time of  
 692 the simulation.

693 As described by the above equations, mass is removed from the surface armour layer  
 694 into the water flowing above. In SSSPAM, mass conservation of the surface armour layer is  
 695 achieved by adding a portion of soil from the 1<sup>st</sup> subsurface layer to the surface armour layer  
 696 equal to the mass entrained into the water flow. It is important to note that the material  
 697 resupplied to the surface armour have the same soil grading as the subsurface layer. So both  
 698 small particles and large particles are resupplied to the armour layer. Most of the time the net  
 699 effect of this material resupply and the size selective erosion will be enrichment of larger  
 700 particles and armour strengthening. Depending on the depth dependent weathering function the  
 701 relative coarseness of the subsurface layers can be less compared to armour layer. But once the  
 702 armour layer is reconfigured with the added material from below and removal of small particles  
 703 through erosion, again the net effect is armour strengthening. More detailed description of this  
 704 process can be found in *Cohen et al.* [2009] and *Welivitiya et al.* [2016].

Formatted: Highlight

Formatted: Highlight

Formatted: Highlight

Formatted: Highlight

Formatted: Font: 12 pt, Not Italic

Formatted: Font: 12 pt, Not Italic

Formatted: Font: 12 pt, Not Italic

Formatted: Font: 12 pt, Not Italic

Formatted: Font: 12 pt, Not Italic

705 -This material resupply propagates down the soil profile (one soil layer supplying  
 706 material to the layer above and receiving material from the layer below) all the way to the  
 707 bedrock layer which is semi-infinite in thickness. Since the soil grading of different layers are  
 708 different to each other, this flux of material through the soil profile changes the soil grading of  
 709 all the subsurface layers. Conceptually the position of the modelled soil column moves  
 710 downward since all vertical distances for the soil layers are relative to the soil surface. In the  
 711 case of deposition the model space would move upwards (discussed in detail later). This  
 712 movement of the “soil model-space” during erosion is illustrated in Figure 2.

713 Note that erosion is limited by the imbalance between sediment transport capacity and  
 714 the amount of the sediment load in the flow as well as the threshold diameter of the particle  
 715 which can be entrained (Shield shear threshold, see *Cohen et al.* [2009] for details) by the water  
 716 flow. These factors limit the potential erosion rate at a pixel. During the test simulations  
 717 presented later in this paper, the depth of erosion  $\Delta h_E$  was always less than the surface armour  
 718 layer thickness  $D_{sur}$  (Figure 2(a)) and the rearrangement of the soil grading of all the layers  
 719 were straightforward. ~~However in the case of deposition, the deposition height  $\Delta h_D$  can exceed  
 720 the surface armour layer thickness (and even the thickness of several soil layers, illustrated in  
 721 Figure 2(b2), (c2), if the timestep is large) and the restructuring of the soil layer grading can be  
 722 complicated. One solution to this problem is to use a smaller timestep. But we preferred to use  
 723 a conceptualization that does not impact as much on the numerical efficiency. Details on  
 724 restructuring the soil column under deposition are given in the following section.~~

### 725 2.3 Sediment deposition

726 If the total mass of incoming sediment  $L_{in}$  is higher than the transport capacity of the  
 727 sediment transport capacity  $T_c$  at the pixel (Table 1, Scenario C) deposition of sediments occurs  
 728 at the pixel. The mass of deposited material is the difference between  $L_{in}$  and  $T_c$ . Although  
 729 calculating the total mass of sediment which needs to deposit at a pixel ( $D$ ) is straightforward,  
 730 determining the distribution of the deposited sediments in the form of deposition mass vector  
 731  $\underline{\Phi}$  is somewhat complicated. The deposition mass vector  $\underline{\Phi}$  depends on the size distribution of  
 732 the incoming sediments which in turn depend on the erosion characteristics of the upstream  
 733 pixels. The calculation of the deposition mass vector  $\underline{\Phi}$  is done using the deposition transition  
 734 matrix  $\mathbf{J}$ . Here  $\underline{\Phi}$  is defined as,

736 
$$\underline{\Phi} = \frac{\underline{\psi}_{in} \mathbf{J}}{\sum J_{z,z} \psi_z} D + \underline{K} \quad (5)$$

735

737 where  $J_{z,z}$  are the diagonal entries of  $\mathbf{J}$  (here and after the subscript  $z$  denotes the  $z^{\text{th}}$  grading  
 738 class), and  $\psi_z$  are the elements of  $\underline{\psi}_{in}$ .  $\underline{K}$  is an adjustment vector which modifies the values in  
 739 deposition mass vector  $\underline{\Phi}$  such that  $\Phi_z \leq \psi_z$ , where  $\Phi_z$  being the elements of the vector  $\underline{\Phi}$ .  
 740 The adjustment vector  $\underline{K}$  ensures that deposited material from each size class is not greater than  
 741 the total amount of sediment load available in the incoming sediment flow and is iteratively  
 742 determined within the deposition module of SSSAPM. The following simplified example  
 743 shows the need to have this adjustment vector and the method we used to calculate it.

Formatted: Font: 12 pt, Not Italic

744 Consider the example values given in Table 2. The total mass of the incoming sediments  
 745 is 75 kg and the sediments are distributed in four size classes. Here the size class one is the  
 746 largest and has the highest potential for deposition (with  $J_{1,1} = 1$ ) while the size class four has  
 747 the lowest potential for deposition (with  $J_{4,4} = 0.1$ ). If the transport capacity  $T_c$  is 40 kg, 35 kg  
 748 of incoming sediments should deposit at the pixel as the total deposition  $D$ . Using the  $\sum J_{z,z} \psi_z$   
 749 value (which is 24) and rescaling these values with  $D$  (total deposition mass), we can calculate  
 750 the masses of sediments which need to be deposited from each grading class. In some cases  
 751 (when the total deposition  $D$  is higher than the  $\sum J_{z,z} \psi_z$  value) the mass of material which  
 752 needs to be deposited can be larger than the available sediments in that particular size class. In  
 753 this example there is 5 kg of sediments in the 1st size class and 10 kg of sediments in the second  
 754 size class respectively. However, our adjusted calculation dictate that there should be 7.29 kg  
 755 deposition from the 1st size class and 10.21 kg from the 2nd size class which is not possible.  
 756 So these values needs to be adjusted to reflect maximum possible deposition from size classes  
 757 one and two which are 5 kg and 10 kg respectively. This adjustment introduces a deficit of 2.5  
 758 kg to the total deposition and it needs to be deposited from the 3<sup>rd</sup> and 4<sup>th</sup> smaller grading  
 759 classes. According to the deposition matrix values  $J_{z,z}$  the deposition probability ratio  
 760 between 3<sup>rd</sup> and 4<sup>th</sup> grading class is 4:1 (0.4:0.1). The deficit mass 2.5kg is deposited from the  
 761 3<sup>rd</sup> and 4<sup>th</sup> size class with 4:1 ratio which accounts to an additional deposition mass of 2 kg  
 762 from 3<sup>rd</sup> size class and 0.5 kg from the 4<sup>th</sup> size class. In this way the entries of the adjustment  
 763 vector  $\underline{K}$  are calculated. Depending on the number of size classes and the distribution of the  
 764 sediments, this adjustment vector  $\underline{K}$  needs to be calculated iteratively.

Formatted: Indent: First line: 1.27 cm

Formatted: Superscript

Formatted: Superscript

765 The deposition of material from the incoming sediment flow reduces the total mass of  
766 the sediment load in the flow and changes its distribution due to this size selective deposition  
767 (particles with higher settling velocity deposit faster). The outflow sediment mass vector  $\underline{\psi}_{out}$   
768 is then calculated by,

$$769 \quad \underline{\psi}_{out} = \underline{\psi}_{in} - \Phi \quad (6)$$

770 Also the deposition height  $\Delta h_D$  is calculated using,

$$771 \quad \Delta h_D = \frac{D}{R_x R_y \rho_s} \quad (7)$$

772  
773 However in the case of deposition, the deposition height  $\Delta h_D$  can exceed the surface  
774 armour layer thickness (and even the thickness of several soil layers, illustrated in Figure 2(b2),  
775 (c2), if the timestep is large) and the restructuring of the soil layer grading can be complicated.  
776 One solution to this problem is to use a smaller timestep. But we preferred to use a  
777 conceptualization that does not impact as much on the numerical efficiency. Details on  
778 restructuring the soil column under deposition are given in the following section.

Formatted: Indent: First line: 1.27 cm

779  
780 The following section describes the methodology for deriving the deposition transition  
781 matrix.

Formatted: Indent: First line: 1.27 cm, Space After: 10 pt

Formatted: Indent: First line: 1.27 cm

### 782 2.3.1 Derivation of deposition transition matrix

783 The deposition transition matrix is derived by considering the particle trajectories at the  
784 pixel level. Assuming all the sediments flowing into the pixel are homogeneously distributed  
785 throughout the water column, we define the critical immersion depth  $h_{ct(z)}$  for all the particle  
786 size classes as illustrated with Figure 3. The critical immersion depth is the vertical distance  
787 travelled by the particle at the average settling velocity of the particle size class  $V_z$  where it will  
788 travel the horizontal distance of the pixel width  $X$  under the flow with the fluid flow velocity  
789  $V_f$  and settle at the far edge (i.e. exit) of the pixel.

$$790 \quad h_{ct(z)} = \frac{X}{V_f} V_z \quad (8)$$

791 Depending on the position of the sediment particle entering into the pixel with respect  
 792 to critical immersion depth, whether or not that particle will deposit in that pixel can be  
 793 determined. Particles entering to the pixel below the critical immersion depth will settle within  
 794 the current pixel, while particles entering above the critical immersion depth will stay in  
 795 suspension and exit the current pixel. The critical immersion depth is greater for larger (or ~~more~~  
 796 ~~dense~~denser) particles and less for smaller (or less dense) particles. For sediment particles in  
 797 larger size classes, the critical immersion depth can be larger than the flow depth  $H_f$  (m)  
 798 (thickness of the water column). That means all the particles in that particle size class will settle  
 799 in the pixel. Using the critical immersion depth and the flow depth we can define the diagonal  
 800 elements  $J_{z,z}$  of the deposition transition matrix **J** in following manner.

$$801 \quad J_{z,z} = \begin{cases} \frac{h_{ct(z)}}{H_f} & \text{for } H_f \geq h_{ct(z)} \\ 1 & \text{for } H_f < h_{ct(z)} \end{cases} \quad (9)$$

802 Note the deposition transition matrix **J** is a diagonal matrix which contains only  
 803 diagonal elements (all off diagonal elements being 0). The evaluation of elements in the  
 804 potential deposition matrix **J** requires the calculation of the critical immersion depth  $h_{ct(z)}$  and  
 805 the flow depth  $H_f$ .

806 The following discussion briefly describes the methodology used to calculate the above  
 807 variables. The average settling velocity of all the particle sizes classes can be calculated for  
 808 typical sediment sizes using Stoke's Law [*Lerman, 1979*].

$$810 \quad V_z = \frac{(\rho_s - \rho_f)g}{18\mu} d_z^2 \quad (10)$$

809  
 811 where  $\rho_s$  and  $\rho_f$  are bulk density of the soil particles and the density of water ( $\text{kg/m}^3$ ) (fluid),  
 812  $g$  is gravitational acceleration ( $\text{m/s}^2$ ),  $d_z$  is the median particle diameter of the size class  $z$  (m)  
 813 and  $\mu$  is the dynamic viscosity of water ( $\text{kg/s/m}^2$ ). The average flow velocity and the flow depth  
 814 can be calculated using the Manning formula [*Meyer-Peter and Müller, 1948; Rickenmann,*  
 815 *1994*]. Although the Manning formula is normally used to calculate the average flow velocity  
 816 in channels, we assume that the same formula can be used to calculate the flow velocity at the  
 817 pixel level assuming water flowing over a pixel as a small channel segment. Manning formula  
 818 states,



819  $V_f = \frac{1}{n} R^{2/3} S^{1/2}$  (11)

820 where  $n$  is the Manning's roughness coefficient,  $R$  is the hydraulic radius (m) and  $S$  is the slope  
 821 (m/m). The Manning's roughness coefficient  $n$  can be approximated using the median diameter  
 822  $d_{50}$  (mm) of the surface armour layer [Coon, 1998] using following equation.

823  $n = 0.034(d_{50})^{1/6}$  (12)

824 The hydraulic radius is the ratio between the cross-sectional area of the flow and the  
 825 wetted perimeter. When we consider the flowing water column at a pixel, the cross-sectional  
 826 area of the flow is the multiplication of flow width (pixel width)  $\omega$  and the flow depth  $H_f$  with  
 827 the wetted parameter being the flow width  $\omega$ . The hydraulic radius at the pixel is then the flow  
 828 depth  $H_f$ . Substituting flow depth for hydraulic radius equation (11) becomes,

830  $V_f = \frac{1}{n} H_f^{2/3} S^{1/2}$  (13)

829

831 The flow velocity at the pixel can be also expressed in terms of upslope contributing  
 832 area  $A_c$ , runoff excess generation  $r$ , flow width  $\omega$  and flow depth  $H_f$ .

833  $V_f = \frac{A_c r}{H_f \omega}$  (14)

834 Solving the equations (13) and (14) the flow depth  $H_f$  and the flow velocity  $V_f$  can be  
 835 calculated in terms of  $A_c$ ,  $r$ ,  $\omega$ ,  $S$  and  $n$  using

836  $H_f = \left( \frac{A_c r n}{\omega S^{1/2}} \right)^{3/5}$  (15)

837  $V_f = \left( \frac{A_c r}{l_c} \right)^{2/5} \left( \frac{S^{3/2}}{n^3} \right)^{1/5}$  (16)

### 838 2.3.2 Restructuring of the soil layers after deposition

839 Deposition of sediment on the soil surface moves the soil surface upwards (soil model-  
 840 space moves upwards). As mentioned earlier the deposition height  $\Delta h_D$  can exceed the surface  
 841 armour layer thickness and/or a number of subsurface soil layer thicknesses. Figure 2(b2)

842 illustrates a typical scenario where the deposition height has exceeded the thickness of the  
843 surface armour layer  $D_{sur}$ .

844 Figure 2(b2) and (c2) shows the movement of the model-space for three soil layers. In  
845 the restructured soil column (Figure 2(c2)) the new 3<sup>rd</sup> layer consists of a portion of the original  
846 layer one (surface armour layer) and the 1<sup>st</sup> original subsurface layer. Because of the upward  
847 movement of the model-space, a portion of the 2<sup>nd</sup> original soil layer and the entire 3<sup>rd</sup> soil layer  
848 has been incorporated into the new bedrock layer. However, the grading of the new bedrock  
849 layer remains unchanged although the material from the original soil layers two and three is  
850 added to the bedrock layer. At the first glance it may seem that this process would drastically  
851 alter the soilscape evolution dynamics by introducing a sharp contrast in soil grading at the  
852 soil-bedrock interface. In SSSPAM a large number of soil layers (50 to 100) are used to ensure  
853 smooth soil grading transition from soil to bedrock.

854 Figure 4 shows three different cases that can occur during the deposition process. In  
855 Case 1 (Figure 4(b)) the deposition height  $\Delta h_D$  is less than the surface armour thickness  $D_{sur}$ .  
856 In Case 2 (Figure 4(c)) the deposition height  $\Delta h_D$  is greater than the surface armour layer  
857 thickness  $D_{sur}$  and the original surface armour layer is situated inside a single new subsurface  
858 layer. Also the new soil subsurface layer which contains the original surface armour layer can  
859 reside in any depth within new soil profile depending on the deposition height (e.g. it can be  
860 1<sup>st</sup>, 2<sup>nd</sup>, 5<sup>th</sup> or any subsurface layer). For simplicity of explanation Figure 4(c) shows this layer  
861 being in the 1<sup>st</sup> new subsurface layer. Case 3 (Figure 4(d)) is similar to the situation in Case 2  
862 where the deposition height  $\Delta h_D$  is greater than the surface armour layer thickness  $D_{sur}$ .  
863 However in this case the original surface armour layer belongs to two new subsurface layers  
864 instead of one. As was with Case 2, the new soil subsurface layers, which contain portions of  
865 the original surface armour layer, can reside at any depth within the new soil profile.  
866 Calculation of soil grading of surface and all the subsurface soil layers are calculated with  
867 different approaches according to previously mentioned deposition scenarios. A detailed  
868 description of these soil grading approaches can be found in Welivitiya [2017].

869 ~~Let the soil grading mass vector of the original soil surface be  $G_{sur}$  and  $G_{sub(1)}$ ,  $G_{sub(2)}$ ,~~  
870 ~~.....,  $G_{sub(n)}$  be the soil grading mass vectors of the original subsurface layers. In the same~~  
871 ~~manner let  $G_{sur}''$  be the soil grading mass vector of the new surface armour layer and  $G_{sub(1)}''$ ,~~  
872  ~~$G_{sub(2)}''$ , ...,  $G_{sub(n)}''$  be the soil grading mass vectors of the new subsurface layers, and  $D_{sur}$~~   
873 ~~and  $D_{sub}$  are the thickness of surface armour layer and the thickness of each subsurface layer~~

Formatted: Default, Space Before: 0 pt, After: 0 pt

874 respectively. Depending on the position of the original surface armour layer in the new soil  
 875 column, different approaches need to be taken in order to calculate the new soil gradings as  
 876 described in following cases.

877 **Case 1:**

878 — In Case 1 (Figure 4(b)) the deposition height  $\Delta h_D$  is less than the surface armour  
 879 thickness  $D_{surf}$ . Considering the uniform soil column cross sectional area, the new soil layer  
 880 mass grading vectors of different soil layers (for Case 1) are calculated as,

881  
 882 
$$\underline{G}_{surf}'' = \underline{\Phi} + \left( \frac{D_{surf} - \Delta h_D}{D_{surf}} \right) \underline{G}_{surf} \quad (17)$$

883 
$$\underline{G}_{sub(i)}'' = \left( \frac{\Delta h_D}{D_{surf}} \right) \underline{G}_{surf} + \left( \frac{D_{sub} - \Delta h_D}{D_{sub}} \right) \underline{G}_{sub(i)} \quad (18)$$

884 
$$\underline{G}_{sub(i)}'' = \left( \frac{\Delta h_D}{D_{surf}} \right) \underline{G}_{sub(i-1)} + \left( \frac{D_{sub} - \Delta h_D}{D_{sub}} \right) \underline{G}_{sub(i)} \quad (19)$$

885  
 886 where  $i$  is the number of new subsurface soil layers such that  $i \in \{2, 3, \dots, n\}$  and  $n$  is the  
 887 number of subsurface layers.

888 **Case 2:**

889 — In Case 2 (Figure 4(c)) the deposition height  $\Delta h_D$  is greater than the surface armour  
 890 layer thickness  $D_{surf}$  and the original surface armour layer is situated inside a single new  
 891 subsurface layer. Also the new soil subsurface layer which contains the original surface armour  
 892 layer can reside in any depth within new soil profile depending on the deposition height (e.g.  
 893 it can be 1<sup>st</sup>, 2<sup>nd</sup>, 5<sup>th</sup> or any subsurface layer). For simplicity of explanation Figure 4(c) shows  
 894 this layer being in the 1<sup>st</sup> new subsurface layer. In the model the original surface armour layer  
 895 is contained in the  $k^{\text{th}}$  new subsurface layer. In this instance the new surface armour layer and  
 896 all the new subsurface layers above  $k^{\text{th}}$  layer will have the same particle size distribution as the  
 897 deposition mass vector  $\underline{\Phi}$ . They are (using the same notation as before),

898  
 899 
$$\underline{G}_{surf}'' = \left( \frac{D_{surf}}{\Delta h_D} \right) \underline{\Phi} \quad (20)$$

900  
 901 
$$\underline{G}_{sub(i)}'' = \left( \frac{D_{sub}}{\Delta h_D} \right) \underline{\Phi} \quad (21)$$

902 where  $i \in \{1, 2, \dots, k-1\}$ .

Formatted: Default

Formatted: Space Before: 0 pt

Formatted: Default

Formatted: Default, Space After: 0 pt

Formatted: Default

Case 2 satisfies the condition  $kD_{sub} \geq \Delta h_D > D_{surf}$ , when the original surface armour layer belongs to a single subsurface layer. The  $k^{th}$  new subsurface layer contains the contribution from three different sources, (1) deposited material, (2) material from the original surface armour layer, and (3) material from the original 1<sup>st</sup> subsurface layer. Using the soil grading mass vectors of these sources the soil grading mass vector of the  $k^{th}$  subsurface layer is,

$$\underline{G}_{sub(k)}'' = \left( \frac{\Delta h_D - D_{surf} - (k-1)D_{sub}}{\Delta h_D} \right) \underline{\Phi} + \underline{G}_{surf} + \left( \frac{kD_{sub} - \Delta h_D}{D_{sub}} \right) \underline{G}_{sub(1)} \quad (22)$$

The soil grading mass vectors of all the other new subsurface layers is,

$$\underline{G}_{sub(i)}'' = \left( \frac{\Delta h_D - (k-1)D_{sub}}{D_{sub}} \right) \underline{G}_{sub(i-k)} + \left( \frac{kD_{sub} - \Delta h_D}{D_{sub}} \right) \underline{G}_{sub(i-k+1)} \quad (23)$$

where  $i \in \{k+1, k+2, \dots, n\}$ .

### Case 3:

Calculation of the soil grading mass vectors for the Case 3 (Figure 4(d)) is similar to Case 2. In this case the deposition height  $\Delta h_D$  is greater than the surface armour layer thickness  $D_{surf}$  and the original surface armour layer belongs to two new subsurface layers. As was with Case 2, the new soil subsurface layers, which contain portions of the original surface armour layer, can reside at any depth within the new soil profile. Figure 4(d) shows the situation where the surface layer now resides in both 1<sup>st</sup> and 2<sup>nd</sup> new subsurface layers. The model assumes that the original surface armour layer is contained in both  $k^{th}$  and  $k+1^{th}$  new subsurface layers. Similar to Case 2 the new surface armour layer and all the new subsurface layers above  $k^{th}$  layer will have the same particle size distribution as the deposition mass vector  $\underline{\Phi}$  and they are calculated using the same equations (20) and (21).

Case 3 (Figure 4(d)) satisfies the condition  $(D_{surf} + kD_{sub}) \geq \Delta h_D > kD_{sub}$ . The new  $k^{th}$  subsurface layer contains the contribution from the deposited material and the material from the original surface armour layer while  $k+1$  layer containing contributions from the original surface armour layer and the first original subsurface layer. The soil grading mass vectors for new  $k^{th}$  layer and  $k+1^{th}$  layer are,

$$\underline{G}_{sub(k)}'' = \left( \frac{\Delta h_D - D_{surf} - (k-1)D_{sub}}{\Delta h_D} \right) \underline{\Phi} + \left( \frac{D_{surf} + kD_{sub} - \Delta h_D}{D_{sub}} \right) \underline{G}_{surf} \quad (24)$$

$$\underline{G}_{sub(k+1)}'' = \left( \frac{\Delta h_D - kD_{sub}}{D_{sub}} \right) \underline{G}_{surf} + \left( \frac{(k+1)D_{sub} - \Delta h_D}{D_{sub}} \right) \underline{G}_{sub(1)} \quad (25)$$

Formatted: Line spacing: 1.5 lines

Formatted: Default

Formatted: Default, Space Before: 0 pt

Formatted: Space Before: 0 pt, After: 0 pt

933 The soil grading mass vectors of all the other new subsurface layers is calculated by,

934 
$$G_{sub(i)}^n = \left( \frac{\Delta h_D - k D_{sub}}{D_{sub}} \right) G_{sub(i-k-1)} + \left( \frac{(k+1) D_{sub} - \Delta h_D}{D_{sub}} \right) G_{sub(i-k)} \quad (26)$$

935 where  $i \in \{k+2, k+3, \dots, n\}$

## 936 2.4 Soil profile weathering

937 The methodology used for simulating the weathering within the soil profile is detailed  
938 by Welivitiya *et al.* [2016]. It ~~used~~ uses a physical fragmentation mechanism where a parent  
939 particle disintegrates into  $n$  number of daughter particles ~~where~~ with a single daughter particle  
940 retaining  $\alpha$ -fraction  $\alpha$  of the parent particle by volume and the remaining  $n-1$  daughter particles  
941 retaining ~~1~~  $1 - \alpha$ -fraction  $1 - \alpha$  of the parent particle volume. By changing  $n$  and  $\alpha$  we can  
942 simulate a wide range of particle disintegration geometries which can be attributed to different  
943 weathering mechanisms. In this paper we used  $n = 2$  and  $\alpha = 0.5$  to simulate symmetric  
944 fragmentation mechanism where a single parent particle breaks down in to 2 equal daughter  
945 particles. But the model can simulate any values of  $n$  and  $\alpha$  which can simulate a wide range  
946 of weathering mechanisms ranging from symmetric fragmentation to granular disintegration.  
947 We decided to use the symmetric fragmentation mechanism based on the results of Wells *et al.*  
948 [2006]. Using the above mentioned parameters, parent - daughter particle diameters and soil  
949 grading distribution values, the weathering transition matrix is constructed according to the  
950 methodology described by Cohen *et al.* [2009] and will not be discussed further.

951 The weathering rate of each soil layer is simulated using a depth dependent weathering  
952 function. It defines the weathering rate as a function of the soil depth relative to the soil surface  
953 depending on the mode of weathering of that particular material. SSSPAM ~~is capable of~~ can  
954 use ~~ing~~ different depth depending weathering functions to simulate the soil profile weathering  
955 rate. For the initial simulations presented in this paper we used the exponential [Humphreys  
956 and Wilkinson, 2007] and humped exponential [Ahnert, 1977; Minasny and McBratney, 2006]  
957 depth dependent weathering functions. Detailed explanation and the rationale of these  
958 weathering functions is presented in Welivitiya *et al.* [2016] and extended by Willgoose [2018].

959 It is important to note that SSSPAM can assign different weathering mechanisms (using  
960 different values of  $n$  and  $\alpha$ -) and different depth dependent weathering functions for each pixel  
961 (node) depending on the material and the dominant weathering drivers (such as temperature)  
962 in the pixels geographical location. Also if need be, the depth dependent weathering function  
963 at each pixel may be changed during the simulation to reflect any perceived temporal change

Formatted: Highlight

Formatted: Highlight

Formatted: Highlight

964 in weathering drivers by slightly modifying the weathering module. This will allow SSSPAM  
965 to conduct simulation studies on global change incorporating both physical and chemical  
966 weathering processes on soilscales in the future.

Formatted: Highlight

### 968 3 SSSPAM simulation setup

969 The objective of the simulations below was to explore the capabilities and implications  
970 of the SSSPAM coupled soilscape-landform evolution model. Although the model is capable  
971 of simulating soilscape and landform evolution for a three-dimensional catchment scale  
972 landform, a synthetic two-dimensional linear hillslope (length and depth) landform was used  
973 here. Because it is two-dimensional, the landform always discharges in a single direction. In  
974 this way the complexities of multidirectional discharge were avoided so we can focus on the  
975 soilscape-landform coupling.

976 ~~Figure 5 shows the synthetic landform used.~~ The simulated landform starts from an  
977 almost flat 1 km long plateau (almost flat area at the top of the hillslope) with a very small  
978 gradient of 0.001% (Figure 5). A hillslope with a gradient of 2.1% starts at the edge of the  
979 plateau and continues 1.5 km horizontally while dropping 31.5 m vertically and terminates at  
980 a valley. The valley (another almost flat area at the bottom of the hillslope) itself has the same  
981 gradient as the upslope plateau (0.001%) and continues for another 1 km. The valley (the  
982 bottom section of the landform) is designed to facilitate sediment deposition so the effect of  
983 sediment deposition on soilscape development can be analysed. The simulated hillslope has a  
984 constant width of 10 m (one pixel wide) and is divided into 350, 10 m long longitudinal  
985 segments with the total number of pixels along slope being 350. At each pixel the soil profile is  
986 defined by a maximum of 102 soil layers. The soil surface armour layer is the topmost soil  
987 layer and it has a thickness of 50 mm. The 100 layers below the surface layer are subsurface  
988 soil layers with a thickness of 100 mm each. The bottommost layer (102<sup>nd</sup> layer) is a permanent  
989 non-weathering layer and it is the limit of the hillslope modelling depth. In this way SSSPAM  
990 is capable of modelling a soil profile with a maximum thickness of 10.05 m. By changing the  
991 number of soil layers used in the simulation SSSPAM is able to simulate a soil profile with any  
992 thickness. However as the number of model layers increases, the time required for the each  
993 simulation also increases. During our initial testing, we found that the soil depth rarely  
994 increased beyond 10 m and decided to set 10.05 m as the maximum soil depth for this initial  
995 scenario.

996 Two soil grading data sets (Table 23) were used for the initial surface soil grading and  
997 the bedrock. The first soil grading was from Ranger Uranium Mine (Northern Territory,  
998 Australia) spoil site. This soil grading was first used by *Willgoose and Riley* [1998] for their  
999 landform simulations. It was also subsequently used by *Sharmeen and Willgoose* [2007] for  
1000 their work with ARMOUR simulations and *Cohen et al.* [2009] for mARM simulation work.  
1001 The soil grading consisted of stony metamorphic rocks produced by mechanical weathering  
1002 with a body fracture mechanism [Wells et al., 2008]. It had a median diameter of 3.5 mm and  
1003 a maximum diameter of 19 mm (Table 2Table 3 - Ranger1a). The second grading was created  
1004 to represent the bedrock ~~using the size classes~~ of the previous soil grading. It contained 100%  
1005 of its mass in the largest particle size class that is 19 mm (Table 2Table 3 - Ranger1b). These  
1006 soil gradings are the same soil gradings used in the SSSPAM parametric study of *Welivitiya et*  
1007 *al.* [2016]. At the start of the simulation the surface armour layer was set to the soil grading  
1008 (Table 2Table 3 - Ranger1a) and all the subsurface layers were set to bedrock grading (Table  
1009 2Table 3 - Ranger1b). The discharge (runoff excess generation) rate of water is derived from  
1010 averaging the 30 year rainfall data collected by *Willgoose and Riley* [1998]. Using the  
1011 simulation setup described above simulations was carried out using the yearly averaged  
1012 discharge rate. For this simulation we set the timestep to 10 years and the model was run for  
1013 10000 timesteps (simulating 100000 years of evolution).

#### 1014 4 Simulation results with exponential weathering function

1015 Figure 6 shows six outputs at different times during hillslope and soil profile evolution.

1016 The upper section in each of the panels in Figure 6 is the cross-section median diameter  
1017 ( $d_{50}$ ) of the soil profile and the landform, with the line denoting the original landform surface.  
1018 The middle panel is the median diameter  $d_{50}$  of the soil surface armour layer. The bottom panel  
1019 is the soil profile relative to the surface highlighting the soil profile  $d_{50}$  (i.e. elevation  
1020 differences at different nodes are removed and the  $d_{50}$  for all the nodes are displayed at the  
1021 dame level). The soil depth is the depth below the surface at which  $d_{50}$  reaches the maximum  
1022 possible particle size (i.e. the bedrock grading). Figure 6(a) shows the initial condition for the  
1023 soilscape: a deep bedrock overlain by a very thin fine-grained soil ~~armour layer~~. The evolution  
1024 of the coupled soilscape and landform at different simulation times are presented in subsequent  
1025 Figures 6(b) - 6(f).

1026 If we initially consider the landform evolution alone, the erosion-dominated regions  
1027 and the deposition-dominated regions can be clearly identified. Initially erosion is highest on

1028 top of the hillslope where the plateau transitions to the hillslope (plateau-hillslope boundary)  
1029 and erosion gradually reduces down the hillslope. Also, there is a sharp increase of surface  $d_{50}$   
1030 at the plateau-hillslope boundary and then a gradual decrease down the hillslope. ~~The transport~~  
1031 ~~capacity of the flow and deposition has the highest erosion (i.e. the rate of change in the~~  
1032 ~~sediment transport capacity) occurring at the top of the hillslope.~~The summit plateau has a  
1033 very low slope gradient and although the contributing area increases across the plateau, the  
1034 potential erosion and the transport capacity of the flow remains negligible resulting in  
1035 minimum erosion. At the plateau-hillslope boundary, the slope gradient suddenly increases.  
1036 This increase in slope gradient and high contributing area increases the potential erosion of the  
1037 flow and causes a rapid increase in transport capacity downslope. This erosion gradually  
1038 reduces further down the hillslope despite increasing contributing area. Although the transport  
1039 capacity increases towards the bottom of the hillslope, water flowing over the downslope nodes  
1040 is laden with sediments already eroded from upslope nodes. This reduces the amount of erosion  
1041 at the downslope nodes.

1042 Turning to the evolution of the soil profile, the upslope plateau retains the initial surface  
1043 soil layer without any armouring due to the very low erosion and it develops a relatively thick  
1044 soil profile as a result of bedrock weathering. The high erosion rate at the plateau-hillslope  
1045 boundary removes all the fine particles from the initial soil layer as well as fine particles  
1046 produced by weathering process, creating a very ~~course~~ coarse surface armour layer. This high  
1047 erosion rate also leads to a relatively shallow soil profile. The erosion rate reduces down the  
1048 slope due to saturation of the flow with sediments from upstream. Low erosion leads to a weak  
1049 armouring and the fine particles produced from surface weathering remain on the surface.  
1050 These processes lead to the fining of the surface soil layer and thickening of the soil profile  
1051 down the hillslope.

1052 With time the location of the high erosion region shifts upstream onto the plateau  
1053 cutting into it. The  $d_{50}$  of the armour layer downslope also decreases. Both of these changes  
1054 occur due to lowering of the slope gradient of the hillslope over time.

1055 Deposition of material occurs on either side of the hillslope-valley boundary. The valley  
1056 at the foot of the hillslope has a very low initial slope gradient. At the hillslope-valley boundary  
1057 (toe slope) the slope gradient reduces suddenly. This sudden slope gradient reduction reduces  
1058 the transport capacity of the water flow and initiates deposition. Initially deposition occurs only  
1059 at the hillslope-valley boundary node and increases its elevation. This deposition and slope



1060 reduction propagates upslope until equilibrium is reached with erosion. Deposition propagates  
1061 across the valley and produces the deposits in the Figure 6.

1062 There is a change in the surface  $d_{50}$  between the erosion and deposition regions starting  
1063 at around 2000 m. The surface  $d_{50}$  of the erosion region reduces down the slope, reaches a  
1064 minimum at 2000 m and then increases as it transitions into the deposition region. This  
1065 can be clearly seen in Figures 6(c) and 6(d). As noted previously the “actual erosion rate”  
1066 reduces down the slope due to saturation of the flow with sediments. At the end of the erosion  
1067 region no more erosion can take place because the flow is completely saturated with sediment.  
1068 Because of the lack of erosion, fine particles are not removed from the surface and weathering  
1069 produces more and more fine particles reducing the surface  $d_{50}$  and increasing the soil depth.

1070 Near the erosion-deposition boundary, only a small amount of sediment is deposited.  
1071 Since the larger particles have the highest probability of deposition, a small amount of coarse  
1072 material deposits there. Downslope into the deposition region the slope further decreases, the  
1073 difference between the transport capacity and the sediment load increases and the rate of  
1074 deposition steadily increases. Since larger particles have a higher probability of depositing first,  
1075 coarse material preferentially deposits. Mixing of these coarse particles with pre-existing  
1076 weathered fine particles produces the observed coarsening of the surface  $d_{50}$ . Once the surface  
1077  $d_{50}$  of the deposition region reaches a peak it starts to decrease again (from 2500 m to 3000 m).  
1078 Beyond 3000 m the deposited material is smaller because the larger particles have already been  
1079 deposited upstream. The deposition of each consecutive downstream node consists with finer  
1080 particles leading to the observed decrease of surface and profile  $d_{50}$ . As expected the soil  
1081 thickness is higher in the deposition regions than the other regions.

1082 With time the deposition region moves upslope. The gradient of  $d_{50}$  observed in earlier  
1083 times of the deposition region (until 30,000 years) decreases and the soil changes into a very  
1084 fine-grained homogeneous material resulting from surface weathering. Due to the high  
1085 weathering rate at the surface and the upper soil layers, the deposited sediment decomposes  
1086 into a very fine material. With time, the  $d_{50}$  of the sediments in the water flow also decreases  
1087 due to low erosion potential and weathering of the surface armour layer of upslope nodes. For  
1088 these reasons the  $d_{50}$  of the deposition region decreases and becomes homogeneous leading to  
1089 burial of the coarse material that was deposited earlier.

1090 The simulation produced a landform morphology which resemble the five unit model  
1091 proposed by Ruhe and Walker [1968]. At the conclusion of the simulation the plateau area

Formatted: Font color: Red

Formatted: Font color: Red

Formatted: Font color: Red

Formatted: Highlight

Formatted: Font color: Auto, Highlight

Formatted: Highlight

Formatted: Font color: Auto, Highlight

Formatted: Font color: Auto, Highlight

Formatted: Highlight

1092 resembles a flat summit, the plateau-hillslope boundary resembles the convex shoulder,  
1093 transition region from the plateau-hillslope boundary to the deposition region resembles the  
1094 backslope with a uniform slope, and the deposition region resembles the concave base divided  
1095 in to upper footslope and lower toeslope. Generally the soil grading distribution is fine at the  
1096 summit, coarsens from the summit to the shoulder and backslope followed by fining from  
1097 backslope to the base [Birkeland, 1984][Birkeland, 1984; Brunner et al., 2004]. Furthermore,  
1098 the soil depth is typically high in summit area, low in shoulder and blacslope, high in upper  
1099 footslope and lower toeslope [Brunner et al., 2004]. The soil grading and the soil depth  
1100 variations of our simulations produces similar trends.

Formatted: Highlight

Formatted: Highlight

Formatted: Highlight

Formatted: Highlight

Formatted: Highlight

Formatted: Highlight

Formatted: Highlight

Formatted: Font color: Auto

Formatted: Indent: First line: 1.27 cm

#### 1102 4.1 Evolution characteristics of different sites

1103 In order to better understand the dynamics of soilscape evolution we also plotted the  
1104 elevation, slope, rate of erosion (and/or deposition), surface  $d_{50}$ , soil depth and profile  $d_{50}$  for  
1105 four sites (Figure 6(a)). The first two sites (sites 1 and 2) are either side of the plateau-hillslope  
1106 boundary in the erosion region. The other two sites (sites 3 and 4) are either side of the  
1107 hillslope-valley boundary in the deposition region.

##### 1108 *Site 1 and 2:*

1109 For site 1 (Figure 7- solid line plots) the erosion and surface  $d_{50}$  are strongly correlated  
1110 over time. The soil depth and profile  $d_{50}$  plots are also highly correlated. The abrupt change in  
1111 profile  $d_{50}$  occurs at the same time as abrupt changes in soil depth. Site 1 initially has small  
1112 erosion because the slope is very low so weathering dominates. This small amount of erosion  
1113 means the elevation and slope are initially constant. Due to the dominance of weathering, both  
1114 surface and profile grading becomes enriched with fine particles and the  $d_{50}$  decreases.  
1115 Weathering of the profile layers creates a relatively deep soil profile. With time the erosion  
1116 front, initially at the plateau-hillslope transition, cuts back into the plateau. The increased  
1117 erosion rate removes the fine material created by weathering leading to a coarse-grained  
1118 armour. This observation may have some important implications for the landform evolution

Formatted: Highlight

1119 modelling community. Most landform evolution models which does not explicitly model soil  
1120 profile evolution or weathering considers a single unchanging soil layer on top of the landform.  
1121 When evolving a landform similar to the setup used in this manuscript, such landform evolution  
1122 models may underestimate upward propagation rate of the erosion front as they will be trying

1123 to erode relatively coarser particles. With weathering producing smaller particles the erosion  
1124 front would propagate faster in a natural hillslope.

1125         When the erosion front crosses site 1, the gradient increases as does the erosion rate (at  
1126 around 20,000 years). During this phase of increasing erosion the surface  $d_{50}$  also increased.  
1127 However, the surface  $d_{50}$  stabilizes around 14 mm before the erosion rate reaches its maximum  
1128 value. This is because once total armouring occurs, the erosion is reduced to a very low value.  
1129 Although the erosion is low, the slope of the site 1 continues to increase until it reaches a  
1130 maximum and the Shield's shear stress threshold diameter also increases. This allows erosion  
1131 to keep increasing while the surface  $d_{50}$  remain essentially constant. When the erosion rate  
1132 overtakes the rate of production of weathering, the soil depth decreases. Increasing erosion  
1133 reduces the soil thickness while coarsening the surface of upper soil layers. This results in the  
1134 increase of the profile  $d_{50}$  at later times. At 20,000 years, the reduction of slope reduces the rate  
1135 of erosion so that, weathering again dominates the site. Weathering produces more fine  
1136 particles reducing the surface  $d_{50}$  from about 48,000 years. The dominance of weathering over  
1137 erosion also increases the soil depth while decreasing the profile  $d_{50}$ .

1138         Both soil depth and profile  $d_{50}$  plots resemble a stair-stepped graph. The reason for this  
1139 appearance is that SSSPAM calculates soil depths as the number soil profile layers. The model  
1140 doesn't interpolate the depth of soil within a single layer. Since the profile  $d_{50}$  is a function the  
1141 soil thickness, this plot also displays this pattern.

1142         For site 2 (Figure 7-dashed line plots) the evolution is simpler than site 1. The initial  
1143 transport capacity and discharge energy at site 2 is very high while the sediment inflow from  
1144 upstream is low because of low erosion from the plateau. The resulting higher erosion rate  
1145 produces a very coarse surface layer and exposes the bedrock in the subsurface. This effect  
1146 causes both the surface  $d_{50}$  and profile  $d_{50}$  to rapidly increase to the maximum possible diameter  
1147 (bedrock grading).

1148         Although the surface  $d_{50}$  has reached the maximum possible diameter the erosion  
1149 continues to increase as the Shield's threshold diameter for entrainment of the water flow has  
1150 increased beyond the maximum particle size (19 mm) and the bedrock grading itself is being  
1151 eroded. However, at around 2,700 years the Shield's threshold diameter decreases below 19  
1152 mm and the fully armoured surface causes the erosion rate to decrease rapidly and becomes  
1153 unstable in time with rapid fluctuations. Once an armour layer develops on the surface, the

1154 profile layers are protected from erosion and weathering becomes more dominant, so the profile  
1155  $d_{50}$  decreases while soil depth increase.

1156 **Site 3 and 4:**

1157 For site 3 (Figures 8-solid line plots) the elevation increases due to deposition. The  
1158 initial increase of surface  $d_{50}$  occurs due to size selective deposition. As noted in the model  
1159 description, larger particles deposit at a higher rate. This deposition of larger particles on the  
1160 surface causes the surface  $d_{50}$  to initially increase.

1161 The subsequent decrease of the surface  $d_{50}$  occurs due to a combination of two  
1162 processes. Firstly, with time the upstream boundary of the deposition region moves upslope  
1163 and since the largest particles tend to deposit at the beginning of the deposition region, the  
1164 sediment flow at site 3 gets enriched with more and more fine particles. Due to the deposition  
1165 of these relatively finer particles the surface  $d_{50}$  tends to decrease. Secondly, weathering of the  
1166 surface and the subsurface layers reduces the surface  $d_{50}$ . Compared to sites 1 and 2 the soil  
1167 depth increase of site 3 is much higher. In sites 1 and 2 the soil profile growth only occurred  
1168 due to the excess of weathering over erosion. At site 3 the soil layer grows due to material  
1169 deposition as well as weathering of the bedrock. The profile  $d_{50}$  increases in the initial stage.

1170 For site 4 (Figures 8-dashed line plots) while the initial evolution is different, in the  
1171 latter stages (beyond year 15,000) the evolution characteristics of the soil properties are similar  
1172 to that of site 3. Since the valley initially has a low slope, the initial erosion is negligible and  
1173 the elevation, slope and erosion remain close to 0. With the growth of the deposition region, a  
1174 “deposition front” moves across the valley. Before the deposition front reaches site 4, the  
1175 elevation, slope and erosion/deposition remain unchanged. Because the initial erosion rate at  
1176 ~~the~~ site 4 is low, there is no armouring so that weathering dominates and the surface  $d_{50}$   
1177 decreases. When the deposition front reaches site 4, the elevation increases due to sediment  
1178 deposition as so does the slope. Due to the size selective deposition of coarse sediment the  
1179 surface  $d_{50}$  increases. Afterwards the evolution of the soil properties is similar to site 3 as the  
1180 same processes are acting at sites 3 and 4.

1181 **5 Simulation results with humped exponential weathering function**

1182 To test the sensitivity of the conclusions in the previous section to changes in the depth  
1183 dependent weathering functions, in this section we explore the effect of weathering using the

1184 humped exponential weathering function. The key difference is that the humped function has  
1185 a low weathering rate at the surface with the peak weathering rate occurring mid-profile.

1186 Superficially, both the humped and exponential weathering functions ~~produce~~  
1187 ~~similar~~produce similar trends, however there are some differences in the particle size  
1188 distribution, soil depth and the evolution of the landform (Figure 9). At identical times the  
1189 surface  $d_{50}$  is coarser and the soil depth is less for the humped simulations. There is also a subtle  
1190 difference in the initial landform evolution. For the exponential weathering function the highest  
1191 erosion rate occurs near the plateau-hillslope boundary (year 2000 near 1,000 m, Figure 6). For  
1192 the humped function this maximum soil surface deviation occurs further down the hillslope  
1193 (year 2000 near 1500 m, Figure 9). For subsequent times, this difference in the location of the  
1194 maximum erosion leads to subtly different landforms.

1195 These differences in landform evolution are explained by the near surface weathering  
1196 rates. For the exponential weathering function the weathering rate is highest at the surface and  
1197 declines exponentially with depth. For the humped exponential weathering function the highest  
1198 weathering rate is at a finite depth below the surface and exponentially decrease below and  
1199 above this depth. Because of the lower surface weathering rate for humped, the surface  $d_{50}$   
1200 remains coarser during the entire simulation. The relative coarseness of the surface means that  
1201 the water flow needs to be more energetic to entrain material from the surface due to the  
1202 Shields's stress entrainment threshold. For the exponential weathering function simulations,  
1203 shear stress of the water flow is high enough to entrain most of the surface soil particles near  
1204 the plateau-hillslope boundary owing to the finer armour layer as a result of surface weathering.  
1205 However for the humped exponential weathering simulations the surface armour is coarser  
1206 because of the lower surface weathering rate and the shear stress of the water flow is not high  
1207 enough to detach material from the armour layer. Because of this, the highest erosion occurs  
1208 downslope where the contributing area is higher and hence the shear stress of the water flow is  
1209 higher.

1210

## 1211 **6 Model and simulation limitations**

1212 Currently the coupled soilsce-landform evolution model SSSPAM, presented here is  
1213 limited in its scientific scope. The model is based on physical fragmentation of parent soil  
1214 particles and it does not model chemical transformations. Also at the current time SSSPAM

Formatted: Font: Bold, Highlight

Formatted: Highlight

Formatted: Font: (Default) Times New Roman, 12 pt, Highlight

Formatted: Highlight

Formatted: Font: (Default) Times New Roman, 12 pt, Highlight

Formatted: Justified, Indent: First line: 1.27 cm, Line spacing: 1.5 lines

Formatted: Highlight



1248 hillslope to run our simulations because, understanding dynamics of 1D hillslope evolution is  
1249 simpler and we can better illustrate possible implications for different processes. Further,  
1250 only limited comparison was done with field data was possible mainly because of a dearth we  
1251 were unable to find any of any experimental work done by any other researchers which has  
1252 using a similar setup as our simulations. However a subsequent paper will deal with  
1253 implications of model results in terms of 4Dimensional one-dimensional and three-dimensional  
1254 alluvial 3Dimensional fluvial fans. In this future manuscript, we compare and contrast the  
1255 model results with experimental work done by authors like Seal et al. [1997], Toro-Escobar et  
1256 al. [2000] and general observation done regarding naturally occurring alluvial fans and their  
1257 formation dynamics.

## 1258 ~~6-7~~ Conclusions

1259 This study presents ~~see at the~~ methodology for incorporating landform evolution into the  
1260 SSSPAM ~~pedogenesis~~ soil grading evolution model. This was achieved by incorporating  
1261 elevation changes produced by erosion and deposition. Previous published work with SSSPAM  
1262 assumed that the landform, slope gradients and contributing areas remained constant during the  
1263 simulation. This did not preclude the landform evolving, only that the soil reached equilibrium  
1264 faster (i.e. had a shorter response time) than the landform evolved (i.e. a “fast” soil, Willgoose,  
1265 2018). In the new version of SSSPAM discussed here, the elevations, contributing area, slope  
1266 gradient and slope directions at each node dynamically evolve. This new model explicitly  
1267 models co-evolution of the soil and the landform, where the response time for soil and landform  
1268 are similar.

1269 By defining “the critical immersion depth”, a novel and simple methodology for size  
1270 selective deposition was introduced to formulate the deposition transition matrix. This  
1271 deposition transition matrix characterises the size selectivity of sediment deposition depending  
1272 on the settling velocity of the sediment particle, with faster settling velocity particles settling  
1273 first.

1274 The results demonstrated SSSPAM’s ability to simulate erosion, deposition and  
1275 weathering processes as well as which govern soil formation and its evolution coupled with an  
1276 evolving landform. The simulation results qualitatively agree with general trends in soil catena  
1277 observed in the field. The model predicts the development of a thin and coarse-grained soil  
1278 profile on the upper eroding hillslope and thick and fine-grained soil profile at the bottom  
1279 valley. Considering the dominant process acting upon the soilscape, the hillslope can be divided

Formatted: Font: (Default) Times New Roman, 12 pt, Highlight

Formatted: Font: (Default) Times New Roman, 12 pt, Highlight

Formatted: Font: (Default) Times New Roman, 12 pt, Highlight

Formatted: Font: (Default) Times New Roman, 12 pt, Highlight

Formatted: Font: (Default) Times New Roman, 12 pt, Highlight

Formatted: Font: (Default) Times New Roman, 12 pt, Highlight

Formatted: Font: (Default) Times New Roman, 12 pt, Highlight

Formatted: Font: (Default) Times New Roman, 12 pt, Highlight

Formatted: Font: (Default) Times New Roman, 12 pt, Highlight

Formatted: Font: (Default) Times New Roman, 12 pt, Highlight

Formatted: Font: (Default) Times New Roman, 12 pt, Highlight

Formatted: Font: (Default) Times New Roman, 12 pt, Highlight

Formatted: Font: (Default) Times New Roman, 12 pt, Highlight

Formatted: Font: (Default) Times New Roman, 12 pt, Highlight

Formatted: Highlight

Commented [rc2]: Is this needed here? It reads like a distraction and also we have added a fudge factor?

Formatted: Font color: Red

Formatted: Font color: Red

Formatted: Font color: Red

1280 into weathering-dominated, erosion-dominated and deposition-dominated sections. The  
1281 plateau (summit) was mainly weathering-dominated due to its very low slope gradient and low  
1282 erosion rate. The upper part of the hillslope was erosion-dominated owing to its high slope  
1283 gradient and high contributing area. The lower part of the hillslope and the valley was  
1284 deposition-dominated. The position and the size of these sections changes with time due to the  
1285 evolution of the landform and the soil profile. During the simulation, the weathering-dominated  
1286 region shrinks due to the erosional region dominating it. The erosion-dominated region expands  
1287 upslope into the previously weathering-dominated region and the downstream boundary  
1288 retreats upslope away from the deposition-dominated region, but shows a net expansion in area.  
1289 The deposition-dominated region expands upslope into the previously erosion-dominated  
1290 region with a net expansion.

1291 The simulation results also show how the interaction of different processes can have  
1292 unexpected outcomes in terms of soilscape evolution. The best example is the fining of the  
1293 surface grading despite an increasing transport capacity and potential erosion rate. This occurs  
1294 due to saturation of the flow with sediment eroded from upstream nodes. Further, the  
1295 comparison of results produced by the exponential and humped exponential weathering  
1296 functions showed how the distribution of weathering rate down the soil profile changes the  
1297 overall properties of the soilscape. For instance, the humped exponential simulation produced  
1298 a thinner soil profile and coarser soil surface armour compared with simulation results of  
1299 exponential weathering function because of the reduced weathering rate at the soil surface. This  
1300 led to a longer-lived surface armour for the humped function.

1301 The synthetic landform simulations demonstrated SSSPAM's ability to qualitatively  
1302 simulate erosion, deposition and weathering processes and to generate familiar soilscales  
1303 observed in the field. Comparison of results obtained from two different depth different  
1304 functions demonstrate how the soilscape dynamic evolution is influenced by the weathering  
1305 mechanisms. This in turn links to the geology of the soil parent material and their preferred  
1306 weathering mechanism which leads to the heterogeneity of soilscape properties in a region. A  
1307 future paper will discuss how this work can be extended to include the impact of chemical  
1308 weathering into soilscape evolution.

## 1309 **7 References**

1310 Agrawal, Y. C., O. A. Mikkelsen, and H. Pottsmith (2012), Grain size distribution and sediment flux  
1311 structure in a river profile, measured with a LISST-SL Instrument, *Sequoia Scientific, Inc. Report*.



1312 Ahnert, F. (1977), Some comments on the quantitative formulation of geomorphological processes in  
1313 a theoretical model, *Earth Surface Processes*, 2(2-3), 191-201, doi:10.1002/esp.3290020211.  
1314 Arya, L. M., and J. F. Paris (1981), A physicoempirical model to predict the soil moisture characteristic  
1315 from particle-size distribution and bulk density data, *Soil Sci. Soc. Am. J.*, 45(6), 1023-1030.  
1316 Behrens, T., and T. Scholten (2006), Digital soil mapping in Germany—a review, *Journal of Plant  
1317 Nutrition and Soil Science*, 169(3), 434-443, doi:10.1002/jpln.200521962.  
1318 Benites, V. M., P. L. O. A. Machado, E. C. C. Fidalgo, M. R. Coelho, and B. E. Madari (2007), Pedotransfer  
1319 functions for estimating soil bulk density from existing soil survey reports in Brazil, *Geoderma*, 139(1-  
1320 2), 90-97, doi:<http://dx.doi.org/10.1016/j.geoderma.2007.01.005>.  
1321 Birkeland, P. W. (1984), *Soils and geomorphology*, Oxford University Press.  
1322 Brunner, A. C., S. J. Park, G. R. Ruecker, R. Dikau, and P. L. G. Vlek (2004), Catenary soil development  
1323 influencing erosion susceptibility along a hillslope in Uganda, *CATENA*, 58(1), 1-22,  
1324 doi:<http://dx.doi.org/10.1016/j.catena.2004.02.001>.  
1325 Bryan, R. B. (2000), Soil erodibility and processes of water erosion on hillslope, *Geomorphology*, 32(3-  
1326 4), 385-415, doi:[http://dx.doi.org/10.1016/S0169-555X\(99\)00105-1](http://dx.doi.org/10.1016/S0169-555X(99)00105-1).  
1327 Carson, M. A., and M. J. Kirkby (1972), Hillslope form and process.  
1328 Chittleborough, D. (1992), Formation and pedology of duplex soils, *Animal Production Science*, 32(7),  
1329 815-825.  
1330 Cohen, S., G. Willgoose, and G. Hancock (2009), The mARM spatially distributed soil evolution model:  
1331 A computationally efficient modeling framework and analysis of hillslope soil surface organization, *J.  
1332 Geophys. Res.-Earth Surf.*, 114, doi:F03001  
1333 10.1029/2008jf001214.  
1334 Cohen, S., G. Willgoose, and G. Hancock (2010), The mARM3D spatially distributed soil evolution  
1335 model: Three-dimensional model framework and analysis of hillslope and landform responses, *J.  
1336 Geophys. Res.-Earth Surf.*, 115, doi:F04013  
1337 10.1029/2009jf001536.  
1338 Coon, W. F. (1998), *Estimation of roughness coefficients for natural stream channels with vegetated  
1339 banks*, US Geological Survey.  
1340 Gessler, P. E., O. Chadwick, F. Chamran, L. Althouse, and K. Holmes (2000), Modeling soil-landscape  
1341 and ecosystem properties using terrain attributes, *Soil Sci. Soc. Am. J.*, 64(6), 2046-2056.  
1342 Gessler, P. E., I. Moore, N. McKenzie, and P. Ryan (1995), Soil-landscape modelling and spatial  
1343 prediction of soil attributes, *International Journal of Geographical Information Systems*, 9(4), 421-432.  
1344 Hillel, D. (1982), *Introduction to soil physics*, Academic Press.  
1345 Hoosbeek, M. R., and R. B. Bryant (1992), TOWARDS THE QUANTITATIVE MODELING OF PEDOGENESIS  
1346 - A REVIEW, *Geoderma*, 55(3-4), 183-210, doi:10.1016/0016-7061(92)90083-j.  
1347 Humphreys, G. S., and M. T. Wilkinson (2007), The soil production function: A brief history and its  
1348 rediscovery, *Geoderma*, 139(1-2), 73-78, doi:<http://dx.doi.org/10.1016/j.geoderma.2007.01.004>.  
1349 Jenny, H. (1941), *Factors of soil formation*, McGraw-Hill Book Company New York, NY, USA.  
1350 Kirkby, M. (1971), Hillslope process-response models based on the continuity equation, *Inst. Br. Geogr.  
1351 Spec. Publ.*, 3(1), 5-30.  
1352 Kirkby, M. (1977), Soil development models as a component of slope models, *Earth surface processes*,  
1353 2(2-3), 203-230.  
1354 Kirkby, M. (1985), A basis for soil profile modelling in a geomorphic context, *Journal of Soil Science*,  
1355 36(1), 97-121.  
1356 Kirkby, M. (2018), A conceptual model for physical and chemical soil profile evolution, *Geoderma*.  
1357 Lerman, A. (1979), *Geochemical processes. Water and sediment environments*, John Wiley and Sons,  
1358 Inc.  
1359 Lin, H. (2011), Three Principles of Soil Change and Pedogenesis in Time and Space, *Soil Sci. Soc. Am. J.*,  
1360 75(6), 2049-2070, doi:10.2136/sssaj2011.0130.

1361 McBratney, A. B., M. L. Mendonça Santos, and B. Minasny (2003), On digital soil mapping, *Geoderma*,  
1362 117(1–2), 3-52, doi:[http://dx.doi.org/10.1016/S0016-7061\(03\)00223-4](http://dx.doi.org/10.1016/S0016-7061(03)00223-4).  
1363 Meyer-Peter, E., and R. Müller (1948), Formulas for bed-load transport, IAHR.  
1364 Minasny, B., and A. B. McBratney (1999), A rudimentary mechanistic model for soil production and  
1365 landscape development, *Geoderma*, 90(1-2), 3-21, doi:10.1016/s0016-7061(98)00115-3.  
1366 Minasny, B., and A. B. McBratney (2006), Mechanistic soil-landscape modelling as an approach to  
1367 developing pedogenetic classifications, *Geoderma*, 133(1-2), 138-149,  
1368 doi:10.1016/j.geoderma.2006.03.042.  
1369 O'Callaghan, J. F., and D. M. Mark (1984), The extraction of drainage networks from digital elevation  
1370 data, *Computer vision, graphics, and image processing*, 28(3), 323-344.  
1371 Parker, G., and P. C. Klingeman (1982), On why gravel bed streams are paved, *Water Resources*  
1372 *Research*, 18(5), 1409-1423, doi:10.1029/WR018i005p01409.  
1373 Rickenmann, D. (1994), An alternative equation for the mean velocity in gravel-bed rivers and  
1374 mountain torrents, paper presented at Proceedings of the ASCE National Conference on Hydraulic  
1375 Engineering.  
1376 Ruhe, R. V., and P. Walker (1968), Hillslope models and soil formation. I. Open systems, *Int Soc Soil Sci*  
1377 *Trans*.  
1378 Salvador-Blanes, S., B. Minasny, and A. B. McBratney (2007), Modelling long-term in situ soil profile  
1379 evolution: application to the genesis of soil profiles containing stone layers, *European Journal of Soil*  
1380 *Science*, 58(6), 1535-1548, doi:10.1111/j.1365-2389.2007.00961.x.  
1381 Schaap, M. G., F. J. Leij, and M. T. van Genuchten (2001), rosetta: a computer program for estimating  
1382 soil hydraulic parameters with hierarchical pedotransfer functions, *J. Hydrol.*, 251(3–4), 163-176,  
1383 doi:[http://dx.doi.org/10.1016/S0022-1694\(01\)00466-8](http://dx.doi.org/10.1016/S0022-1694(01)00466-8).  
1384 Scull, P., J. Franklin, O. Chadwick, and D. McArthur (2003), Predictive soil mapping: a review, *Progress*  
1385 *in Physical Geography*, 27(2), 171-197.  
1386 Seal, R., C. Paola, G. Parker, J. B. Southard, and P. R. Wilcock (1997), Experiments on downstream fining  
1387 of gravel: I. Narrow-channel runs, *Journal of hydraulic engineering*, 123(10), 874-884.  
1388 Sharmeen, S., and G. R. Willgoose (2006), The interaction between armouring and particle weathering  
1389 for eroding landscapes, *Earth Surface Processes and Landforms*, 31(10), 1195-1210,  
1390 doi:10.1002/esp.1397.  
1391 Sharmeen, S., and G. R. Willgoose (2007), A one-dimensional model for simulating armouring and  
1392 erosion on hillslopes: 2. Long term erosion and armouring predictions for two contrasting mine spoils,  
1393 *Earth Surface Processes and Landforms*, 32(10), 1437-1453, doi:10.1002/esp.1482.  
1394 Sommer, M., H. Gerke, and D. Deumlich (2008), Modelling soil landscape genesis—a “time split”  
1395 approach for hummocky agricultural landscapes, *Geoderma*, 145(3), 480-493.  
1396 Strahler, A. H., and A. N. Strahler (2006), *Introducing physical geography*, J. Wiley.  
1397 Tarboton, D. G. (1997), A new method for the determination of flow directions and upslope areas in  
1398 grid digital elevation models, *Water resources research*, 33(2), 309-319.  
1399 Temme, A. J., and T. Vanwalleghem (2015), LORICA—A new model for linking landscape and soil profile  
1400 evolution: Development and sensitivity analysis, *Computers & Geosciences*.  
1401 Toro-Escobar, C. M., C. Paola, G. Parker, P. R. Wilcock, and J. B. Southard (2000), Experiments on  
1402 downstream fining of gravel. II: Wide and sandy runs, *Journal of Hydraulic Engineering*, 126(3), 198-  
1403 208.  
1404 Vanwalleghem, T., U. Stockmann, B. Minasny, and A. B. McBratney (2013), A quantitative model for  
1405 integrating landscape evolution and soil formation, *Journal of Geophysical Research: Earth Surface*,  
1406 118(2), 331-347, doi:10.1029/2011JF002296.  
1407 Welivitiya, W. D. D. P. (2017), A next generation spatially distributed model for soil profile dynamics  
1408 and pedogenesis, University of Newcastle, Australia, University of Newcastle, Australia.  
1409 Welivitiya, W. D. D. P., G. R. Willgoose, G. R. Hancock, and S. Cohen (2016), Exploring the sensitivity  
1410 on a soil area-slope-grading relationship to changes in process parameters using a pedogenesis model,  
1411 *Earth Surf. Dynam.*, 4(3), 607-625, doi:10.5194/esurf-4-607-2016.

1412 Wells, T., P. Binning, G. Willgoose, and G. Hancock (2006), Laboratory simulation of the salt weathering  
1413 of schist: I. Weathering of schist blocks in a seasonally wet tropical environment, *Earth Surface*  
1414 *Processes and Landforms*, 31(3), 339-354, doi:10.1002/esp.1248.  
1415 Willgoose, G. (2018), *Principles of Soilscape and Landscape Evolution*, Cambridge University Press.  
1416 Willgoose, G., R. L. Bras, and I. Rodriguez-Iturbe (1991), A coupled channel network growth and  
1417 hillslope evolution model: 1. Theory, *Water Resources Research*, 27(7), 1671-1684,  
1418 doi:10.1029/91wr00935.  
1419 Willgoose, G., and S. Riley (1998), The long-term stability of engineered landforms of the Ranger  
1420 Uranium Mine, Northern Territory, Australia: Application of a catchment evolution model, *Earth Surf.*  
1421 *Process. Landf.*, 23(3), 237-259, doi:10.1002/(sici)1096-9837(199803)23:3<237::aid-esp846>3.0.co;2-  
1422 x.  
1423 Willgoose, G., and S. Sharmeen (2006), A One-dimensional model for simulating armouring and  
1424 erosion on hillslopes: I. Model development and event-scale dynamics, *Earth Surface Processes and*  
1425 *Landforms*, 31(8), 970-991, doi:10.1002/esp.1398.  
1426 Yoo, K., and S. M. Mudd (2008), Toward process-based modeling of geochemical soil formation across  
1427 diverse landforms: A new mathematical framework, *Geoderma*, 146(1-2), 248-260,  
1428 doi:<http://dx.doi.org/10.1016/j.geoderma.2008.05.029>.  
1429 Zhang, G.-H., L.-L. Wang, K.-M. Tang, R.-T. Luo, and X. Zhang (2011), Effects of sediment size on  
1430 transport capacity of overland flow on steep slopes, *Hydrological Sciences Journal*, 56(7), 1289-1299.

1431  
1432  
1433  
1434  
1435

**Figure 1**

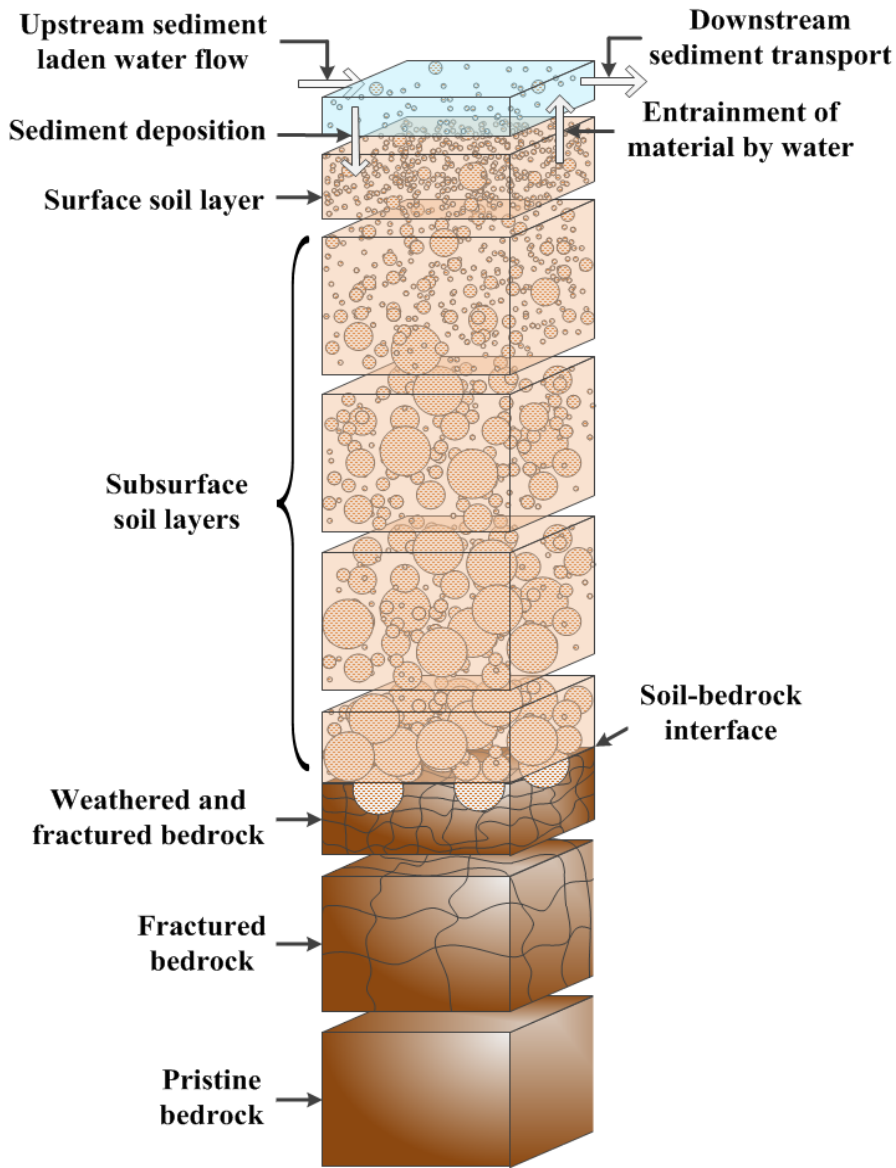


**Figure 1** Schematic diagram of the SSSPAM model.

**Figure 2**

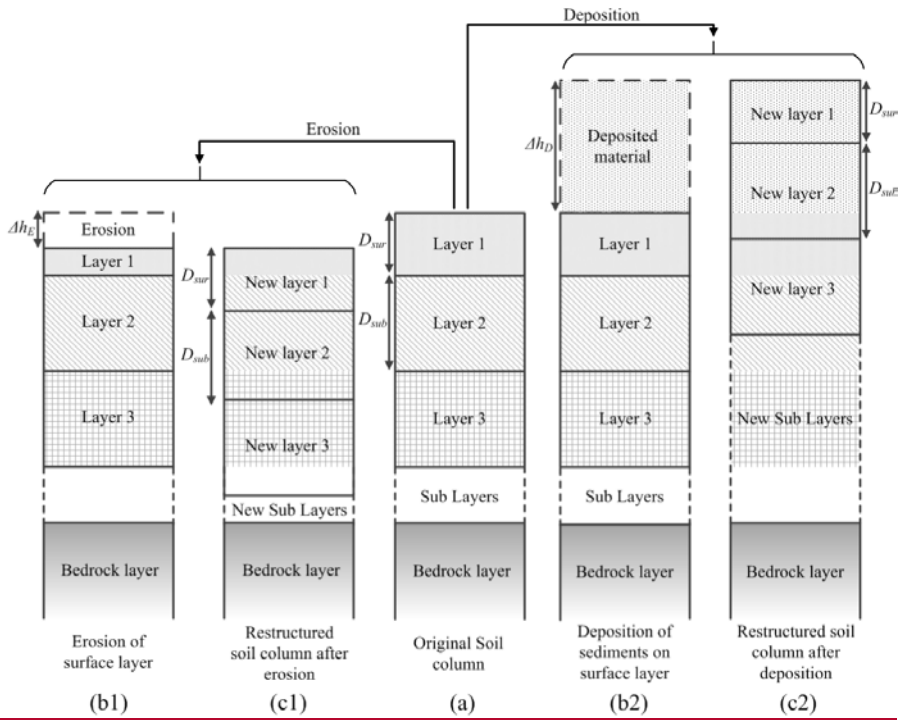


**Figure 2** Erosion, Deposition and the restructuring of the soil profile (a) original soil profile, (b1, c1) for erosion, (b2, c2) for deposition.

1441  
1442  
1443  
1444  
1445  
1446  
1447  
1448  
1449  
1450  
1451  
1452  
1453  
1454

1455  
1456  
1457  
1458  
1459  
1460  
1461  
1462  
1463  
1464  
1465  
1466  
1467  
1468  
1469  
1470  
1471  
1472  
1473  
1474

**Figure 3**

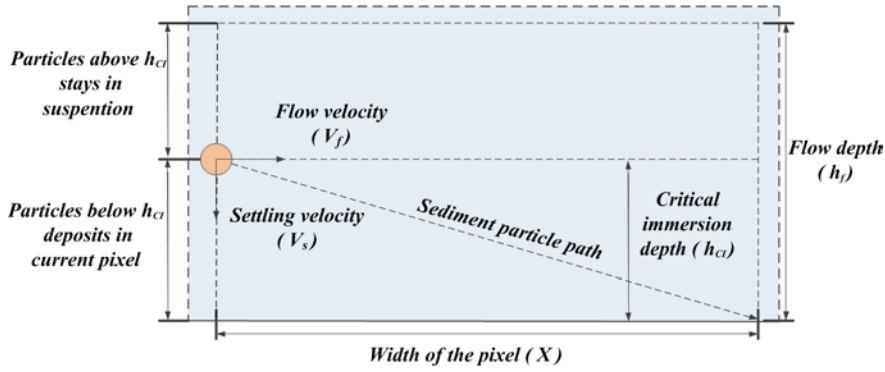
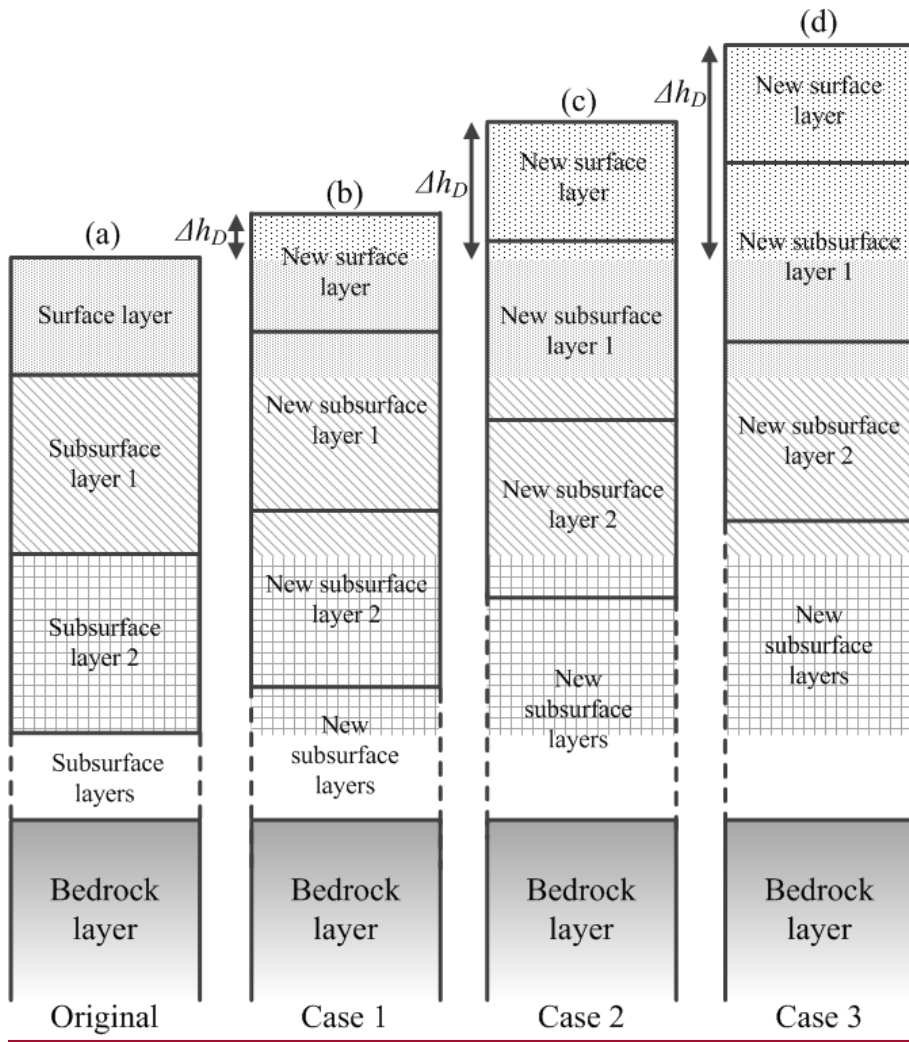


**Figure 3** Determination of critical immersion depth of a sediment particle

1475

**Figure 4**



1476

**Figure 4** Different deposition scenarios

1477

1478

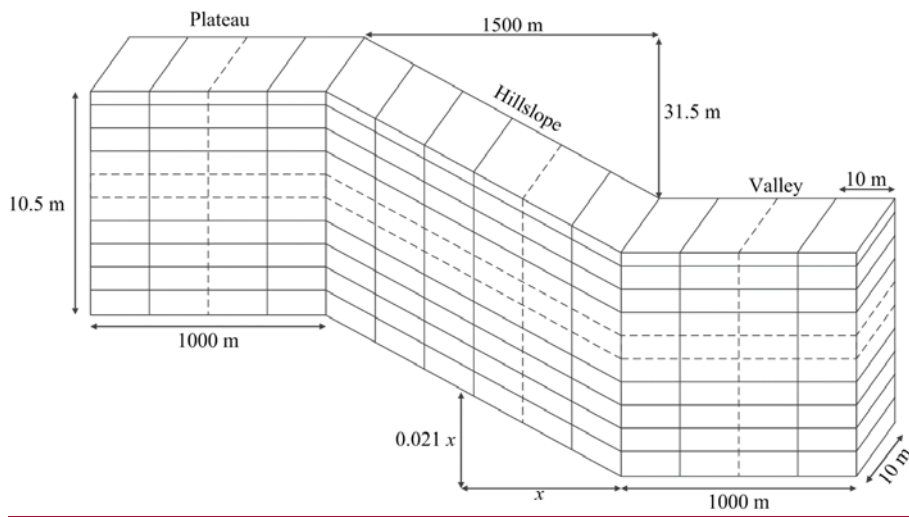
1479

1480

1481

1482  
1483

**Figure 5**



1484

**Figure 5** The simulated landform and the definition of nodes.

1485

1486

1487

1488

1489

1490

1491

1492

1493

1494

1495

1496

1497

1498

1499

**Figure 6**



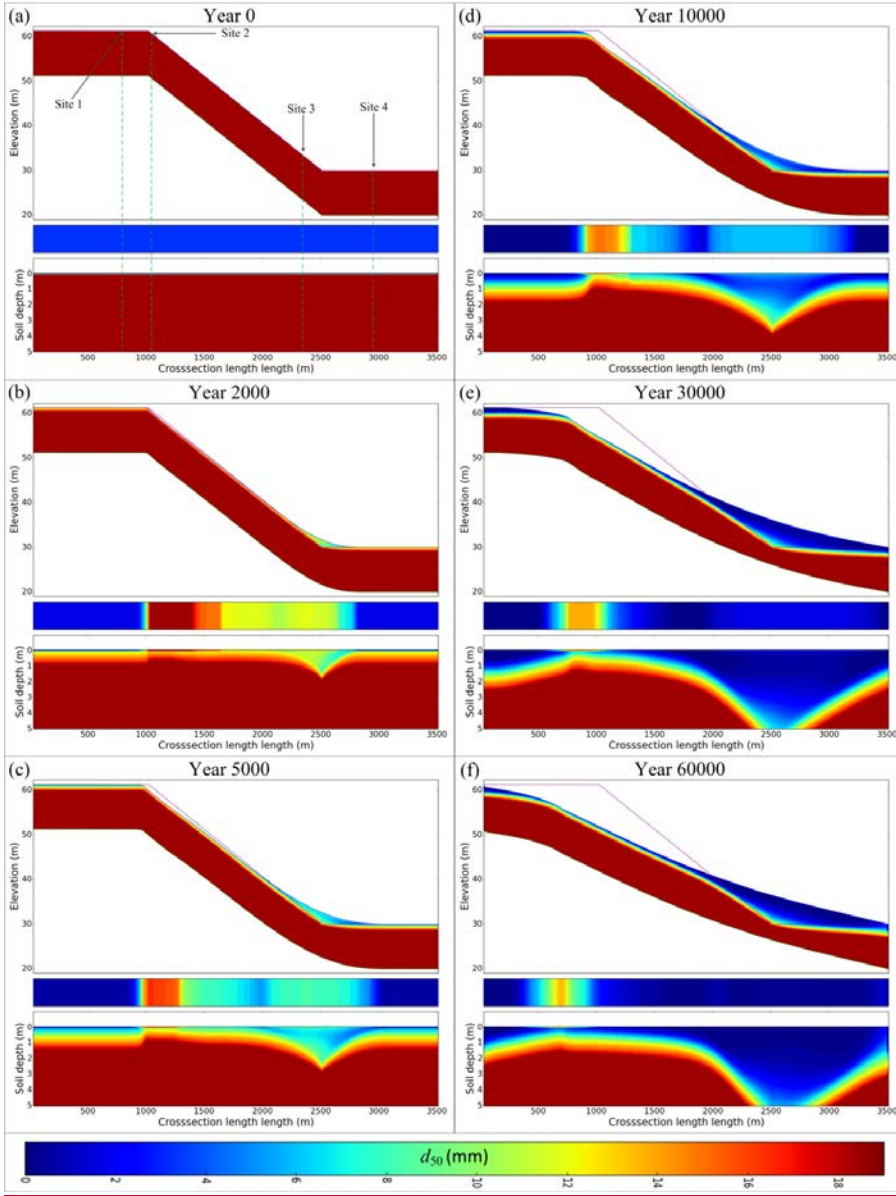


**Figure 6** Evolution of the soilscape with the exponential depth dependent weathering function.

**Figure 6**

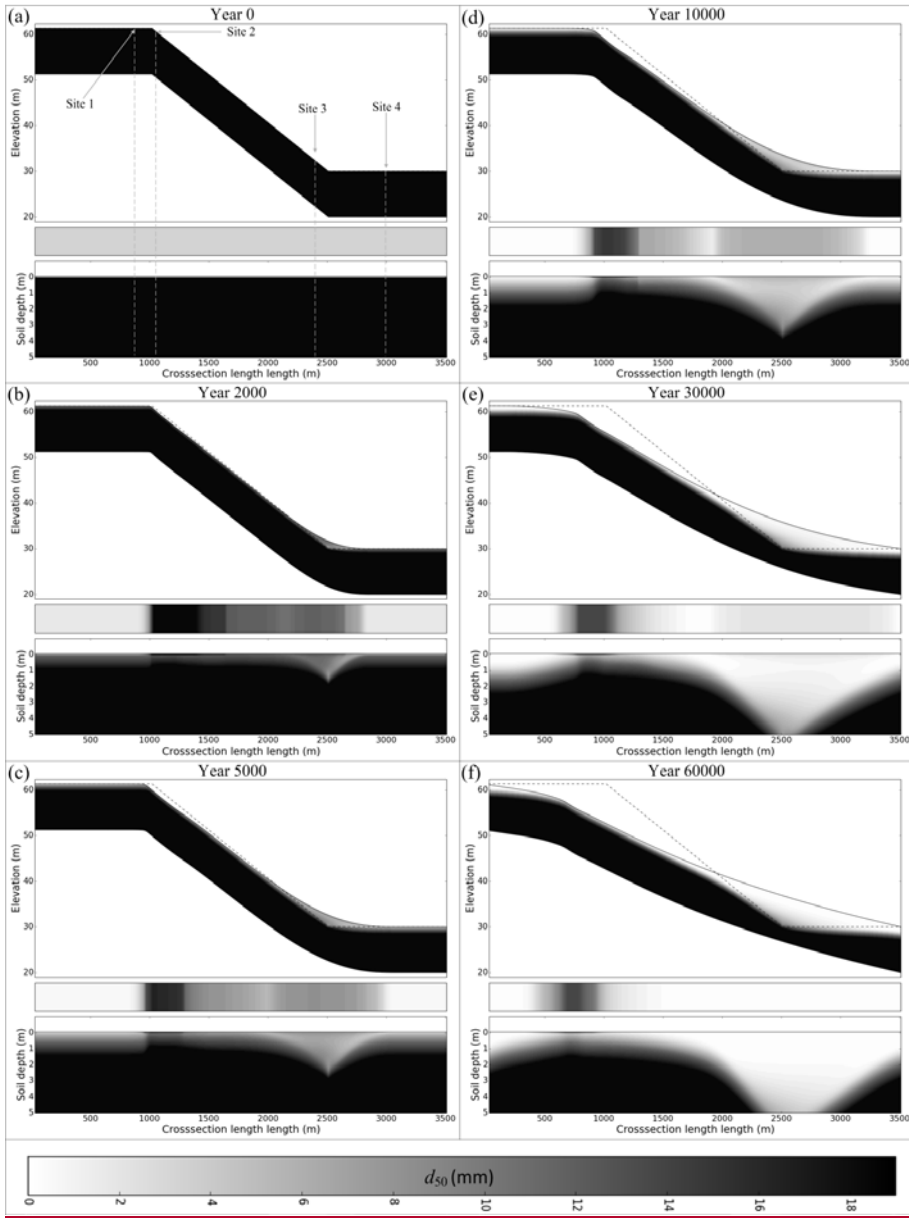
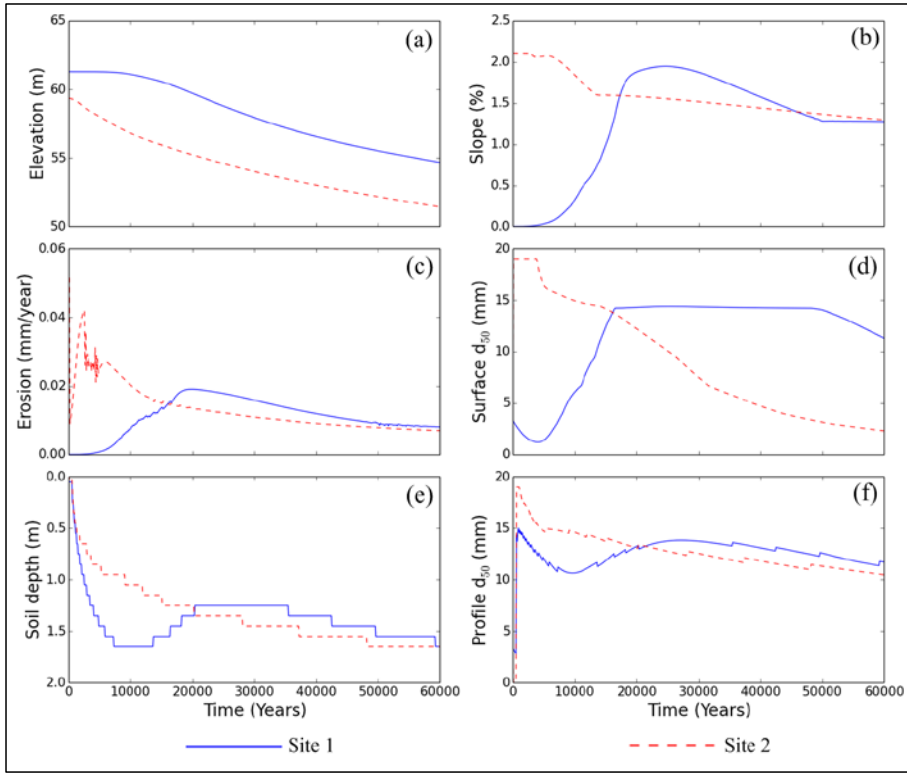


**Figure 6** Evolution of the soilscape with the exponential depth dependent weathering function.

1505  
1506  
1507  
1508  
1509

1510

**Figure 7**



1511

**Figure 7** Evolution characteristics of Sites 1 and 2, (a) elevation, (b) hillslope gradient, (c) erosion rate, (d) surface  $d_{50}$ , (e) soil depth, and (f) profile  $d_{50}$ .

1514

1515

1516

1517

1518

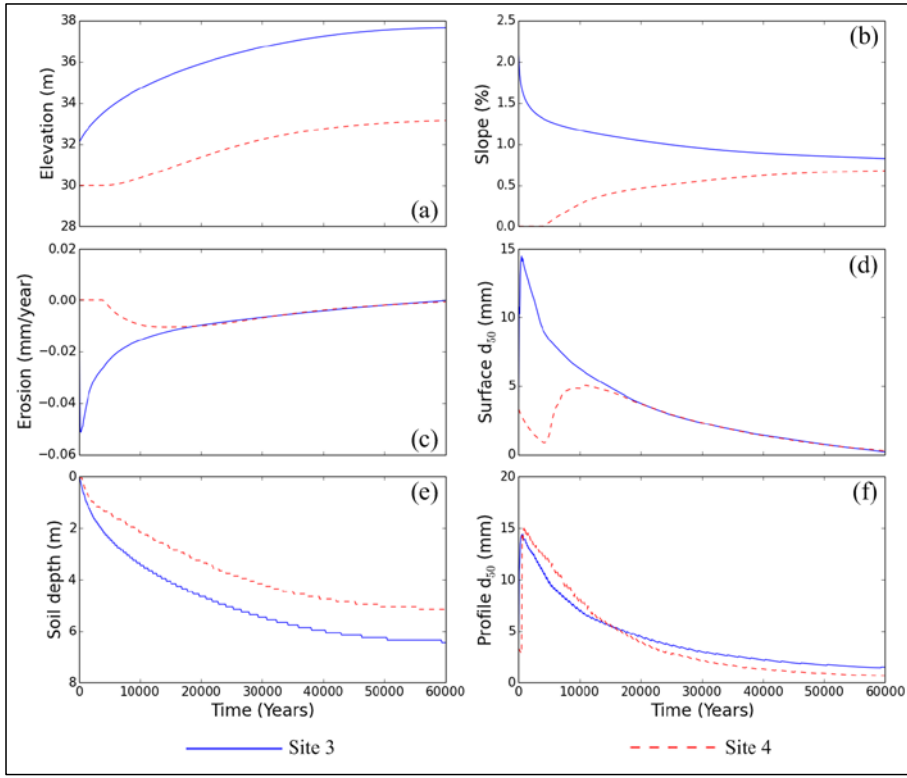
1519

1520

1521

1522

**Figure 8**



1523

1524 **Figure 8** Evolution (near the hillslope-valley boundary) of Sites 3 and 4. (a) elevation, (b)  
 1525 hillslope gradient, (c) erosion rate, (d) surface  $d_{50}$ , (e) soil depth, and (f) profile  $d_{50}$ .

1526

1527

1528

1529

1530

1531

1532

1533

1534

1535

**Figure 9**

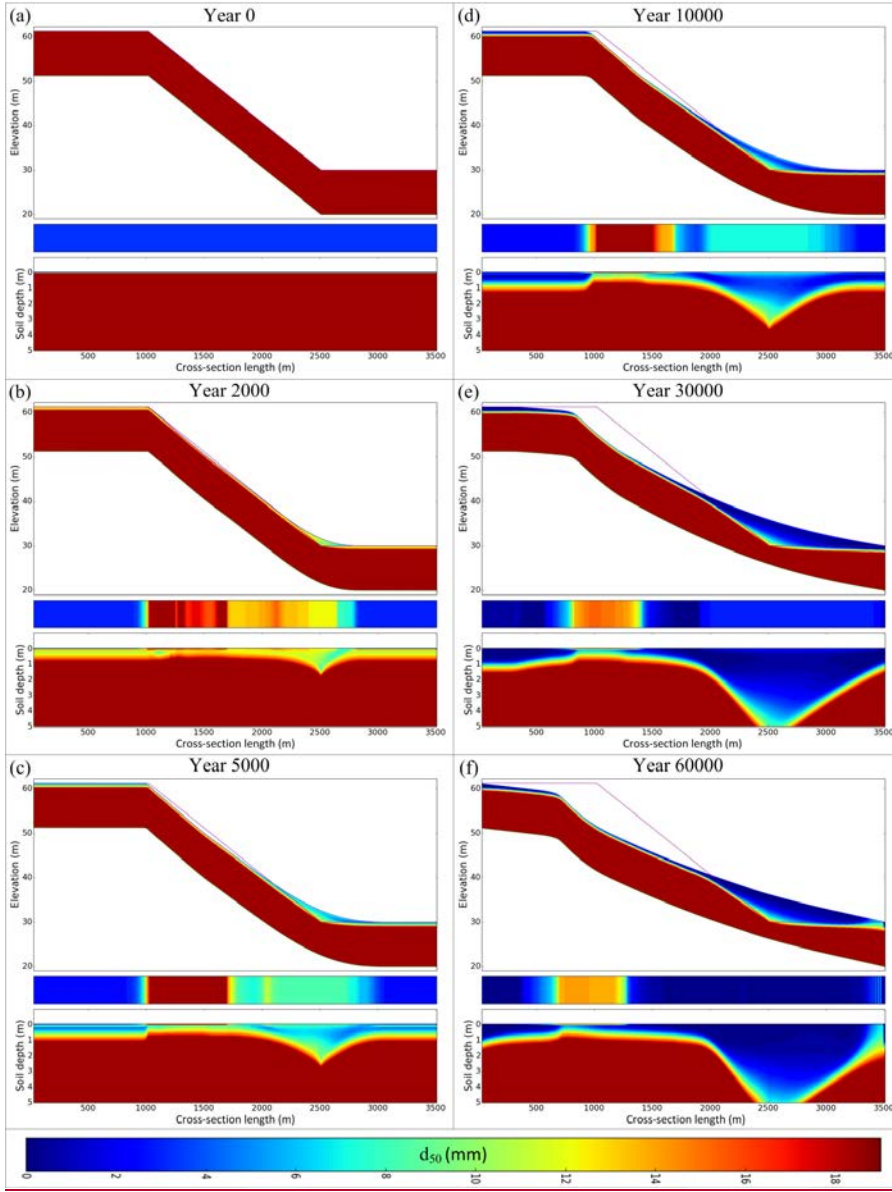


**Figure 9** Evolution of the soilscape with the humped exponential depth dependent weathering function.

**Figure 9**

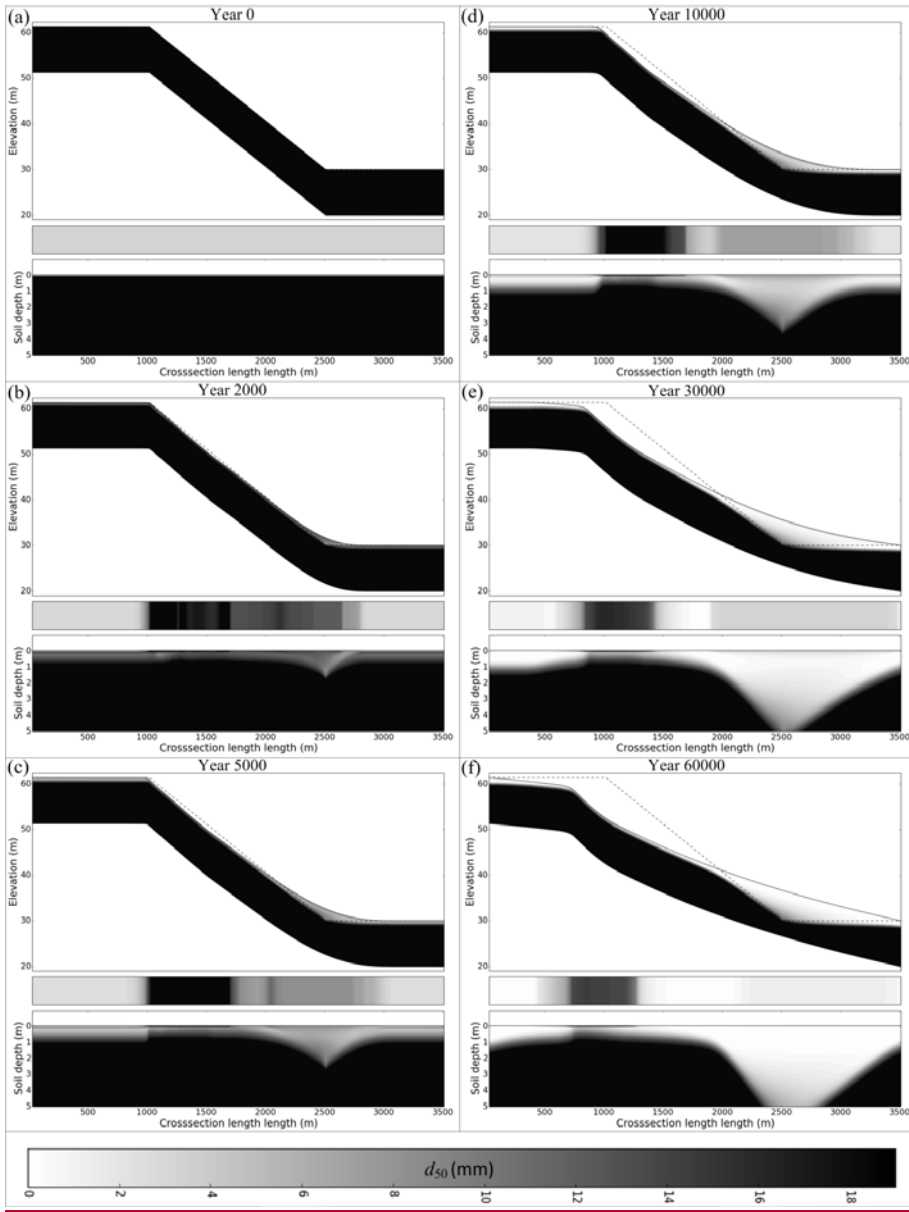


**Figure 9** Evolution of the soilscape with the humped exponential depth dependent weathering function.

**Table 1** Determination of erosion and deposition

1546  
1547  
1548  
1549  
1550  
1551  
1552  
1553  
1554  
1555  
1556  
1557  
1558  
1559  
1560  
1561  
1562

<u>Scenario</u>	<u>Condition</u>	<u>Actual erosion</u> $E_a (kg s^{-1})$	<u>Deposition</u> $D (kg s^{-1})$
<u>A</u>	$L_{in} + E_p < T_c$	$T_c - L_{in}$	$\underline{0}$
<u>B</u>	$L_{in} + E_p \geq T_c$	$E_p$	$\underline{0}$
<u>C</u>	$L_{in} \geq T_c$	$\underline{0}$	$L_{in} - T_c$

1563

**Table 2** Example calculation of adjustment vector  $K$ .

<u>Size Class</u>	<u>Elements of <math>\psi_{in}</math> (<math>\psi_z</math>)</u>	<u>Entries of <math>J</math> (<math>J_{z,z}</math>)</u>	<u><math>J_{z,z} \psi_z</math></u>	<u>Adjusted <math>J_{z,z} \psi_z</math></u>	<u>Deficit / Surplus</u>	<u>Diagonal elements of <math>K</math></u>	<u>Entries of <math>\Phi</math></u>
<u>1</u>	<u>5.00</u>	<u>1.0</u>	<u>5.00</u>	<u>7.29</u>	<u>-2.29</u>	<u>-2.29</u>	<u>5.00</u>
<u>2</u>	<u>10.00</u>	<u>0.7</u>	<u>7.00</u>	<u>10.21</u>	<u>-0.21</u>	<u>-0.21</u>	<u>10.00</u>
<u>3</u>	<u>20.00</u>	<u>0.4</u>	<u>8.00</u>	<u>11.67</u>	<u>8.33</u>	<u>2.00</u>	<u>13.67</u>
<u>4</u>	<u>40.00</u>	<u>0.1</u>	<u>4.00</u>	<u>5.83</u>	<u>34.17</u>	<u>0.50</u>	<u>6.33</u>
<u>Total</u>	<u>75.00</u>		<u>24.00</u>	<u>35.00</u>			<u>35.00</u>

1564

1565

1566

1567

1568

1569

1570

1571

1572

1573

1574

1575

1576

1577



1578  
1579  
1580  
1581  
1582  
1583  
1584

**Table 3 Soil grading distribution data used for SSSPAM simulation.**

<u>Grading Range (mm)</u>		<u>Ranger1a</u>	<u>Ranger1b</u>	
<u>0</u>	<u>:</u>	<u>0.063</u>	<u>1.40 %</u>	<u>0.0%</u>
<u>0.063</u>	<u>:</u>	<u>0.111</u>	<u>2.25 %</u>	<u>0.0%</u>
<u>0.111</u>	<u>:</u>	<u>0.125</u>	<u>0.75 %</u>	<u>0.0%</u>
<u>0.125</u>	<u>:</u>	<u>0.187</u>	<u>1.15 %</u>	<u>0.0%</u>
<u>0.187</u>	<u>:</u>	<u>0.25</u>	<u>1.15 %</u>	<u>0.0%</u>
<u>0.25</u>	<u>:</u>	<u>0.5</u>	<u>10.20 %</u>	<u>0.0%</u>
<u>0.5</u>	<u>:</u>	<u>1</u>	<u>9.60 %</u>	<u>0.0%</u>
<u>1</u>	<u>:</u>	<u>2</u>	<u>12.50 %</u>	<u>0.0%</u>
<u>2</u>	<u>:</u>	<u>4</u>	<u>16.40 %</u>	<u>0.0%</u>
<u>4</u>	<u>:</u>	<u>9.5</u>	<u>20.00 %</u>	<u>0.0%</u>
<u>9.5</u>	<u>:</u>	<u>19</u>	<u>24.60 %</u>	<u>100.0%</u>